Spatial Pressure Distribution on the Finger Pad During Tactile Sensing of Cylindrical Shapes

by

Louis H. Buell Jr.

B.S. Mathematics, Morehouse College, 1999
B.S. Electrical Engineering, Georgia Institute of Technology, 1999

Submitted to the Department of Electrical Engineering and Computer Science
in Partial Fulfillment of the Requirements for the Degree of

Master of Science in Electrical Engineering and Computer Science

at the
Massachusetts Institute of Technology
February 2003

Author.....
Department of Electrical Engineering and Computer Science
January 17, 2003

Certified by.....
Dr. Mandayam A. Srinivasan
Senior Research Scientist
Thesis Supervisor

Accepted by.....
Arthur C. Smith
Chairman, Committee on Graduate Students
Department of Electrical Engineering and Computer Science

Spatial Pressure Distribution on the Finger Pad During Tactile Sensing of Cylindrical Shapes

by

Louis H. Buell

Submitted to the Department of Electrical Engineering and Computer Science
on January 17, 2003, in Partial Fulfillment of the
Requirement for the Degree of Master of Science in
Electrical Engineering and Computer Science

ABSTRACT

The sense of touch aids humans in determining the physical properties of objects such as surface texture, shape, and softness. The force distribution on the skin in contact with an object is the primary stimulus to the human tactile system. In this study, the spatial distribution of normal pressure on the surface of the finger pad in contact with cylindrical objects was measured using a sensitive pressure sensor array that was purchased from a vendor (Pressure Profile Systems, Inc.). Effects of object curvature and contact force on the pressure distribution were studied. Deconvolution, a signal processing technique, was used in an attempt to increase the spatial resolution of the empirical data.

The characteristics of the pressure sensor array were determined first by using a 3-axis motion platform and a high precision single axis motor to apply controlled stimuli. The behavior of individual elements of the pressure sensor array were examined for drift, repeatability, linearity and anisotropy. In addition, sensitivity to spatial positioning of the stimulus and inter-element variability were also studied. The sensor response was shown to be approximately linear and anisotropic, and the gain for each element of the sensor was variable. The sensor elements were calibrated to convert voltages to pressures.

The pressure distribution on the skin surface of 5 subjects was measured when cylindrical objects of two different diameters were indented onto the finger pad. A single sensor element was moved in small increments relative to the contact region to see if smaller step size between measurements produced better results. The correlation between the pressure distribution and the fingerprint was also studied. Dips in surface pressure roughly corresponded to grooves in the fingerprint, though these features were at the limit of the spatial resolution of the sensor. The pressure records were compared with the pressure distribution predicted by Hertz theory of contact mechanics. Hertz theory was found to model the observed pressure distribution reasonably well, though it failed to account for observed anisotropy and pressure concentration due to finger ridges.

To improve the limited spatial resolution of the pressure sensor, application of deconvolution was investigated. Deconvolution was not able to increase the spatial resolution of pressure measurements enough to fully resolve pressure concentrations due to individual finger ridges. This was most likely due sensor noise and the complexity of the spatial response profile of the pressure sensor.

Thesis Supervisor: Dr. Mandayam A. Srinivasan
Title: Senior Research Scientist

Acknowledgements

I would like to thank my thesis advisor, Srini, for giving me the opportunity to be a part of the Touch Lab family. Thank you for your guidance, support and patience.

I would like to thank James and Raju for their contributions, assistance, and guidance on this research project. I couldn't have done it without the help of both of you.

I would like to thank my lab mates Hyun, Jung, Lihua, Suiren, David, Mannivan, Wan-Chen, Ning, Emerson, Boon, and Monica for helping make the Touch Lab such a positive and productive environment.

I would like to thank my family and friends for their support.

Contents

1.0 Introduction

1.1 Overview

The human body has the ability to interact with the outside world through the use of five sensory systems: touch, sight, sound, smell and taste. The information received from these senses is important for human beings to function, and undoubtedly, touch plays a significant role in many aspects of life. The tactile sense aids humans in gathering information about physical properties of objects, such as the shape, size, softness, temperature and texture. Furthermore, this sensory system allows humans to manipulate or grasp objects and to feel pain or pleasure. Although researchers have a comparatively advanced understanding of how humans see and hear, little is understood about the complex mechanisms involved in touch.

While scientists know that touch receptors are located throughout the skin and are constantly supplying information about surrounding environments, further research is necessary to establish a complete knowledge of the mechanics involved in touch. As a result, the primary goal of this research project is to provide a clearer understanding of the biomechanics of the human tactile system and how humans perceive objects through touch. We know that the following events take place during a human's perception of an object through touch: 1) an object comes into contact with the finger resulting in a distribution of forces on the surface of the skin; 2) the surface force distributions lead to internal mechanical stresses and strains; 3) the mechanoreceptors in the skin transduce the stresses and strains into neural impulses; and 4) the object is perceived when neural impulses reach and are decoded by the brain [Raju and Srinivasan, 1999]. Figure 1-1 illustrates these steps.

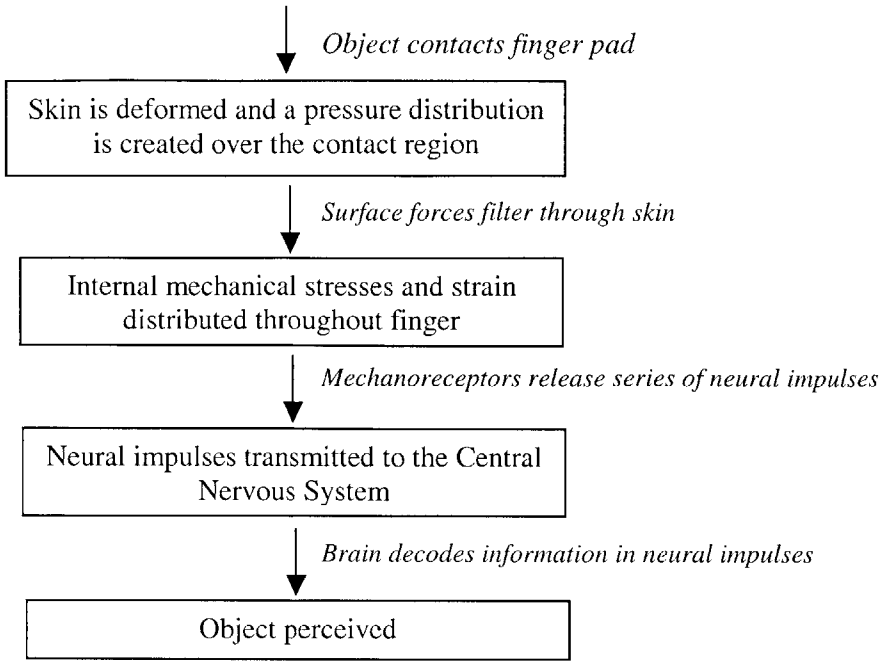

Figure 1-1. The events that take place during a human's perception of an object through touch.

1.2 Motivation

This study will focus on measuring the pressure distribution on the surface of the finger when it comes in contact with an object, the first step of Figure 1-1. Understanding the relationship between the shape of an object indented onto the finger pad and the resulting surface pressure distribution during touch is essential to understanding how humans perceive an object by touch. A study of the pressure distribution on the surface of the finger pad will give us further insight into the distribution of stresses and strains on the mechanoreceptors.

In previous work, Finite Element Models (FEM) have been used to study the pressure distribution when surfaces of different curvatures are indented onto the fingertip. However, these models need to be verified with empirical measurements to ensure their validity. The present study will allow researchers to compare our empirical

measurements with FEM predictions of surface traction and thus adjust the model parameters to better reflect reality. This will allow us to check a step in the tactile sensing transduction pathway that we have only been able to model so far. Thus, our study will provide further fundamental scientific understanding of the origins and mechanisms of tactile information.

Another long term goal of our study of fingertip pressure distribution is to aid in the development of tactile sensors for hand and arm prostheses that will give the user a sense of touch. This research can also allow researchers to improve tests to evaluate tactile sensibility of normal and impaired hands. Understanding the pressure distribution will also provide insights for the design and development of tactile sensors for dexterous robots which perform human-like functions in unstructured environments.

1.3 Thesis Overview

This thesis is organized as follows: Background information about the anatomy of the finger as well as previous research about the biomechanics of the human tactile system are presented in Chapter 2. Chapter 3 describes the experimental setup and the pressure sensor used to collect pressure measurements. The results of measuring the pressure distribution of the finger pad are introduced in Chapter 4. Chapter 5 concludes the paper with a summary of the results.

2.0 Background

2.1 Human Fingertip

The human finger tip is comprised of bone, nail, blood vessels, fat, nerves, sweat glands and skin. The skin of the human finger pad is made of an epidermis and a dermis layer. The epidermis is the outer layer of the body that protects it from the outside environment. It is comprised of a number of layers: stratum corneum, stratum lucidum, stratum granulosum, malphigian layer, and stratum basale [Tubiana, 1981]. The upper-most layer of the epidermis is made up of dead skin cells that are easily removed, and a series of ridges that make up the fingerprint are located on the surface of the epidermis. The dermis is located below the epidermis and protects and cushions the body. It houses sweat glands, hair follicles, blood, lymph vessels and nerve endings. The dermis and epidermis interdigitate in a pattern that mimics the surface ridges on the skin [Lockhart et al., 1965]. Near this interface four types of mechanoreceptors are located: Merkel's disks, Meissner's corpuscles, Pacinian corpuscles, and Ruffini corpuscles [Johansson and Vallbo, 1983]. These mechanoreceptors gather information about the features of objects, and also sense pressure, pain, and temperature.

2.2 Previous Work

Tactile research can be separated into three distinct areas: biomechanics, psychophysics, and neurophysiology. Biomechanical studies deal with understanding the mechanics of touch, and the resulting stress-strain relationships in the skin, which in turn activate the mechanoreceptors that send neural impulses to the brain. Neurophysiological studies deal with the coding of tactile information into neural impulses. Psychophysical studies explore the behavioral response of the brain to a physical stimulus.

This research project deals primarily with the biomechanical area of tactile research. Research on the biomechanics of tactile sensing involve investigation of the mechanical properties of skin, the surface pressure during contact, and the stress-strain relationship that occurs in the skin. In previous research in this area, Philips and Johnson modeled the finger as a homogeneous, linear elastic, isotropic and infinite medium and studied the connection between neurological readings and the strain beneath the surface of the finger [Philips and Johnson, 1981b]. Srinivasan proposed the *waterbed model* of the finger, which modeled the finger as an elastic membrane filled with an incompressible fluid, and predicted the deformation profile on the surface [Srinivasan, 1989]. Gulati and Srinivasan measured the force response of the human finger pad to indentation with shaped objects and proposed a model to mathematically represent this response [Gulati and Srinivasan, 1996]. Dandekar and Srinivasan created a multi-layered FEM model of the fingertip that was able to determine the surface deformation and stress-strain relation during touch [Dandekar and Srinivasan, 1996]. Diane Pawluk measured the spatially distributed pressure response and force of the dynamic interaction between a flat indentor and the finger pad [Pawluk, 1997]. Cysyk and Srinivasan also created a multi-layered FEM model of the human finger pad The finger pad was indented with surfaces of various curvatures and they found that the object curvature was directly proportional to the surface pressure distribution [Cysyk, 1999]. Raju and Srinivasan investigated the mechanics of touch using a multi-layered FEM of a primate finger pad and addressed the problem of computing surface loads from neural responses. They showed that the surface pressure could be decoded from neural impulses [Raju and Srinivasan, 1999].

2.3 Hertz Theory

Hertz theory of normal contact of elastic solids predicts the shape of the area of contact when two non-conforming solids touch [Johnson, 1985]. This theory of the contact between two elastic bodies applies to homogeneous, isotropic bodies that are much larger than the contact area. When two smooth nonconforming surfaces initially come in contact, they touch at a single point. As the load increases, deformation occurs in the

area of that point, the area of contact grows, and so does the distribution and magnitude of surface tractions. During this process, Hertz theory predicts the shape and area of contact, as well as the distribution and magnitude of surface tractions over the surface. As a benchmark to compare with our empirical data, we used Hertz theory to predict the surface pressure distribution of the fingertip when it comes in contact with cylindrical objects of various radii.

The relative radius of curvature of the two contacting bodied is given by

$$\frac{1}{R} = \frac{1}{R_1} + \frac{1}{R_2} \tag{2.1}$$

where R_1 is the radius of the finger pad and R_2 is the radius of the contacting object. When the finger and object come in contact, with a known load P, the resulting contact area has a radius of,

$$a = \left(\frac{3PR}{4E^*} \right)^{1/3} \tag{2.2}$$

where

$$\frac{1}{E^*} = \frac{1-\nu_1^2}{E_1} + \frac{1-\nu_2^2}{E_2} \tag{2.3}$$

E_1 is the modulus of elasticity of finger pad and E_2 is the modulus of elasticity of the object. ν_1 is the Poisson's Ratio for the human finger pad, and ν_2 is the Poisson's Ratio of the object. If the object is incompressible, then the Poisson's Ratio is assumed to be 0.5. The Poisson's Ratio of the finger pad was assumed to be 0.48 [Srinivasan and Dandekar, 1996].

Assuming that the contact area is circular and has radius a and load P, then the maximum

contact pressure (p_0) is given by,

$$p_0 = \left(\frac{3P}{2\pi a^2}\right) = \left(\frac{6PE^{*2}}{\pi^3 R^2}\right)^{1/3} \tag{2.4}$$

The pressure distribution produced is of the form

$$p = p_0\left\{1-\left(r/a\right)^2\right\}^{1/2} \tag{2.5}$$

where r is the radial distance from the contact center and $r \le a$.

2.4 Deconvolution of Shift-Invariant Sensor

Ridges, sweat pores, and grooves in the finger print are all features that may have interesting consequences for the mechanics of touch. In order to study the effects of such fine features, measurements with fine spatial resolution are required. Deconvolution is one potential method for increasing the spatial resolution of interfacial pressure measurements.

Deconvolution is the inverse of convolution, a familiar signal processing technique. In deconvolution an input signal *x[n]* is estimated from a measured output signal *y[n]*, when the impulse response *h[n]* of a system is known. Successful deconvolution depends on linearity and shift invariance of the system, as well as low noise, and accurate knowledge of the system impulse response. Figure 2-1 gives a block diagram of the system to be deconvolved in this study. Here the goal is recover the actual finger pad pressure distribution from the measured finger pad pressure distribution, using the spatial response profile of the sensor.

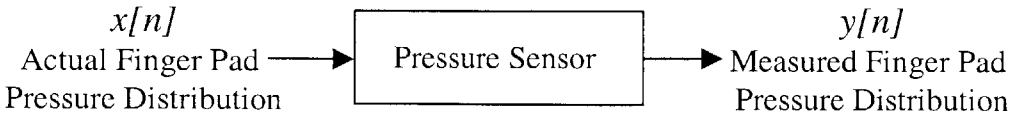

Figure 2-1. Block diagram of the surface pressure measurement of the finger pad.

A shift-invariant system is one in which a spatial shift in the input corresponds to an identical shift in the output (analogous to time invariance). In order for a system to be shift-invariant the curvature of the body must be constant [Raju and Srinivasan, 1999]. Accordingly, we limited our study to indentation by cylindrical stimuli, in which curvature remains constant with shifts in spatial coordinate. A second requirement for shift invariance is that fixed boundary conditions must not be near where shift-invariance is evaluated Accordingly, we made our measurements near the center of the pressure sensor, far from the fixed boundary condition of zero pressure outside the array.

3.0 Finger Pad Pressure Distribution Measurement System

3.1 Experimental Setup

The apparatus designed to measure the surface pressure of the finger pad consists of a motion platform, a load cell, a pressure sensor, various indentors and a personal computer (PC). Figure 3-1 shows the experimental setup. The motion platform consists of two Daedal High Precision Linear Tables each with a Zeta 57 step motor. One axis travels in the x while the other axis in the y direction in a Cartesian plane. A third Zeta 57 step motor is used for a rotational direction of travel. A Sensotec 1000 gram Model 31 Miniature load cell is used to measure the total net force that was applied to the fingertip. The data from the load cell is collected by a Sensotec Model HM Single Channel Signal Conditioner/Indicator with RS232 input to a PC. A highly sensitive tactile pressure sensor is used to measure pressure data from the finger pad, which is then sent through a NuDAQ ACL-8111 Multi-Function Data Acquisition Card into the PC. A C++ program was used to control the motion platform and to record data from the load cell and pressure sensor.

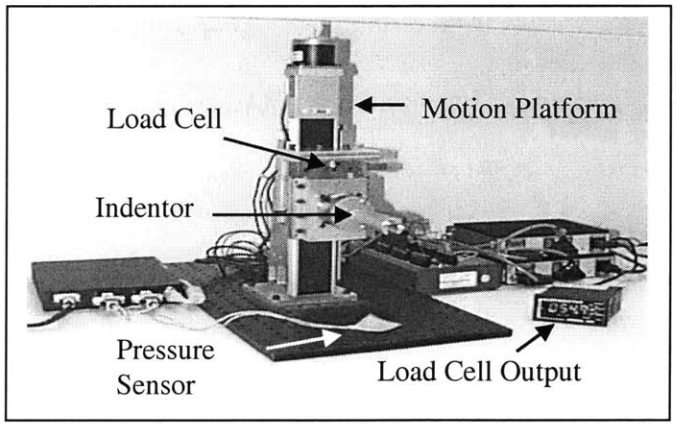

Figure 3-1. Finger Pad Pressure Distribution Measurement System. Consists of highly sensitive pressure sensor, motion platform to control movement of stimulus, load cell to record net force, and various sized interchangeable cylindrical indentors.

The cylinders used to indent the finger pad are attached to the rotational motor during experiments. In order to measure the total net force applied to the fingertip, two sets of 500 gram weights are used to counterbalance the mass of the rotational motor against the load cell using pulleys. When a load is applied to the finger pad by the indentor, the motor compresses the load cell and the force applied is measured. We assume there is no torque because motor is attached to linear bearings. Figure 3-2 shows a schematic of the system used to measure the net force applied to the finger pad.

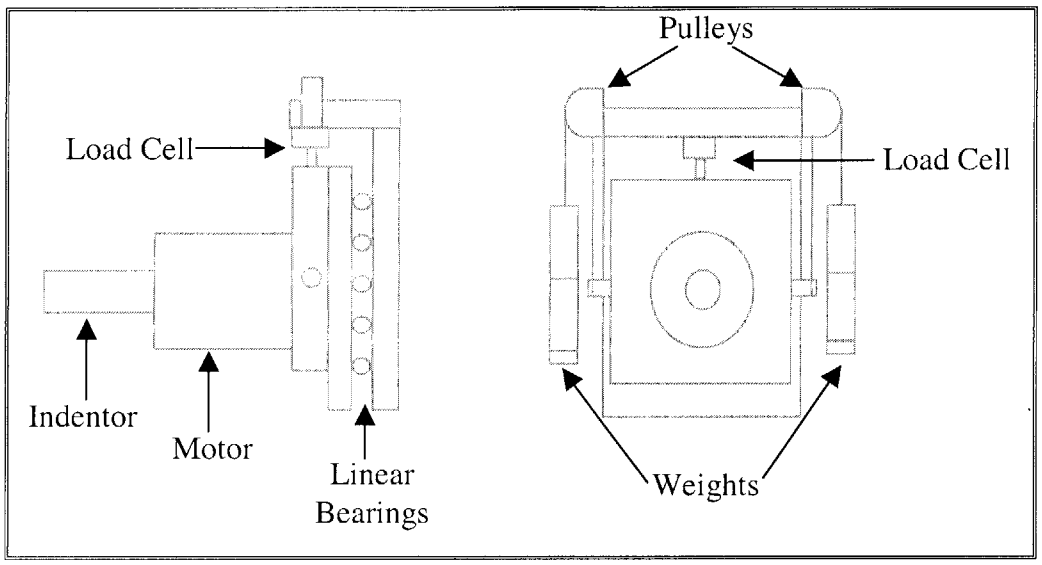

Figure 3-2. Schematic of the system used to measure the net force applied to the finger pad, which consists of an indentor, motor, load cell, two pulleys, and two sets of weights. The weights are used to counterbalance the mass of the rotational motor against the load cell in order to directly measure the load applied to the finger pad.

Cylinders of various radii were used to indent the fingertip during experiments. The first cylinder had a 1 inch diameter while the second had a ½ inch diameter. The conformable pressure sensor was attached to each cylindrical indentor with double sided tape. The subject's hand was supported in a plastic mold with the index finger positioned at 30° degrees from the horizontal, so that the most sensitive part of the fingertip contacted the object. The hand and forearm were constrained and the fingernail was glued to the mold to prevent finger pad movement.

3.2 Pressure Sensor

In order to obtain the surface pressure distribution of the finger pad, we used a highly sensitive tactile pressure sensor developed by Pressure Profile System Inc in Los Angeles, California. The sensor consists of an array 8 elements by 7 elements or 56 total elements; with the size of each element measuring 2 mm by 2 mm. The space between each element is approximately 0.005 inches or 0.127 mm wide. This sensor is conformable and able to fit around various shaped objects. Figure 3-3 shows both sides of the outside of the sensor. The gray side is used as the contacting surface because its response provides less noisy measurements.

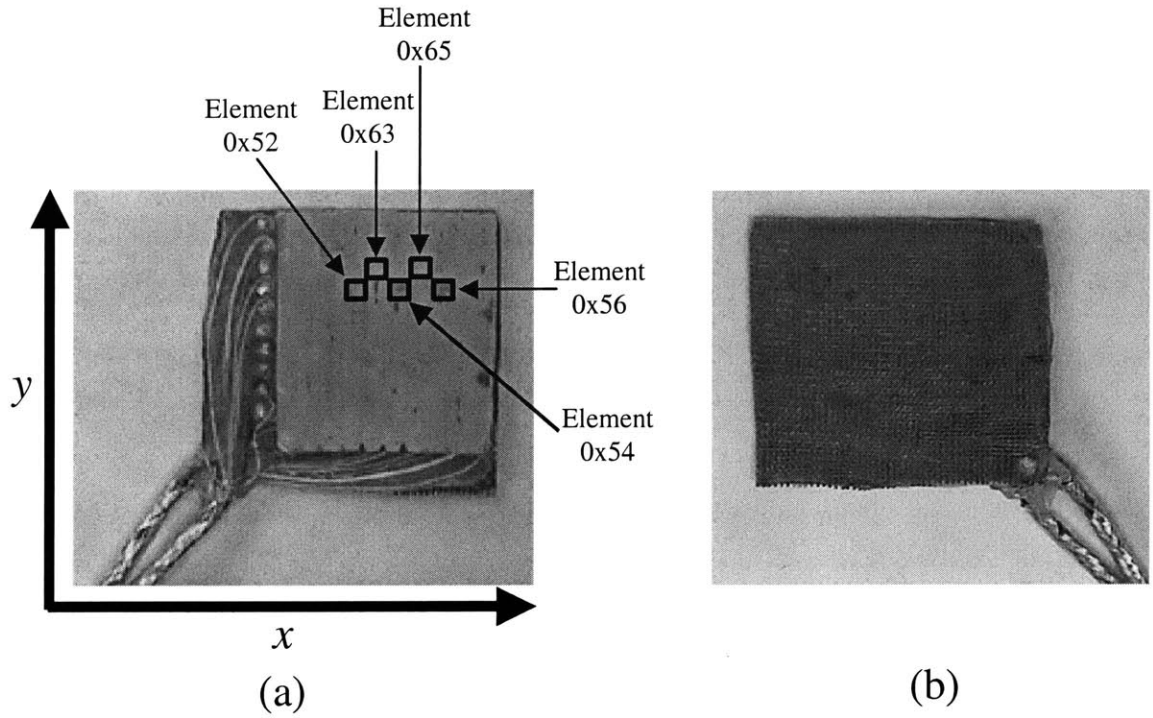

Figure 3-3. Picture of both sides of the pressure sensor. (a) Coordinate system (x and y direction specified) used to study the characteristics of the sensor, as well as the location of five elements is marked. (b) The gray side of the sensor is used as the contacting surface.

The sensor uses capacitive sensing. It is made of a set of parallel strips of copper, which are separated by silicone rubber spaces and orthogonal to another set of parallel strips of

copper. The air in-between the two strips of copper is used as a dielectric or a nonconductor of direct electric current. Each intersection of the parallel copper strips constitutes an element. When pressure is applied to the sensor exterior, the copper strips are pressed together, thus increasing the capacitance of the element. This change in capacitance is proportional to the change in pressure above the element [Pawluk, 1997]. Figure 3-4 shows the design of the sensor.

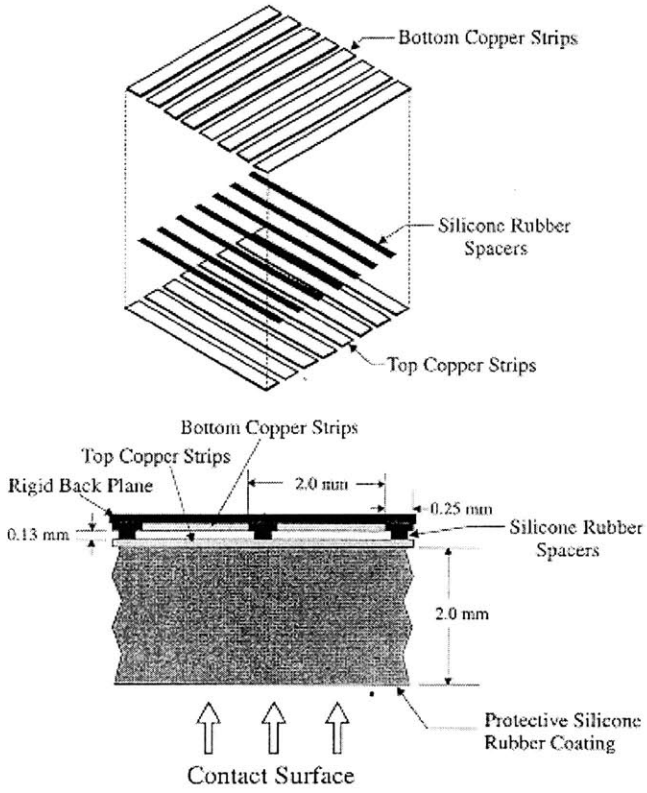

Figure 3-4. Capacitive pressure sensor design [adapted from Pawluk, 1997].

3.3 Sources of Error in Pressure Measurement

We designed several experiments to study the characteristics of the pressure sensor. The characteristics we studied were drift, time dependence, repeatability, linearity, anisotropy, and inter-element variability.

3.3.1 Drift

The pressure sensor was found to exhibit drift in its measurements. Drift was measured over a 10 hour period with the sensor stationary and unloaded. We collected data from the sensor every 30 seconds for 10 hours. Figure 3-5 shows the resulting drift of the sensor. For the first hour, the sensor measurements decrease, and we called this the warm up period for the sensor electronics. During the next three hours the sensor measurements are flat. All experiments that were performed to collect finger pad pressure measurements (see chapter 4) were performed during this three hour time period. In the last 6 hours the sensor measurements steadily increase and we avoided taking finger pad pressure measurements after the four hour mark. In order to account for the drift in our experimental measurements, for each data point, we collected data from the sensor with no load and then data with the prescribed load. We then subtracted the two measurements to calculate the change in voltage or change in pressure.

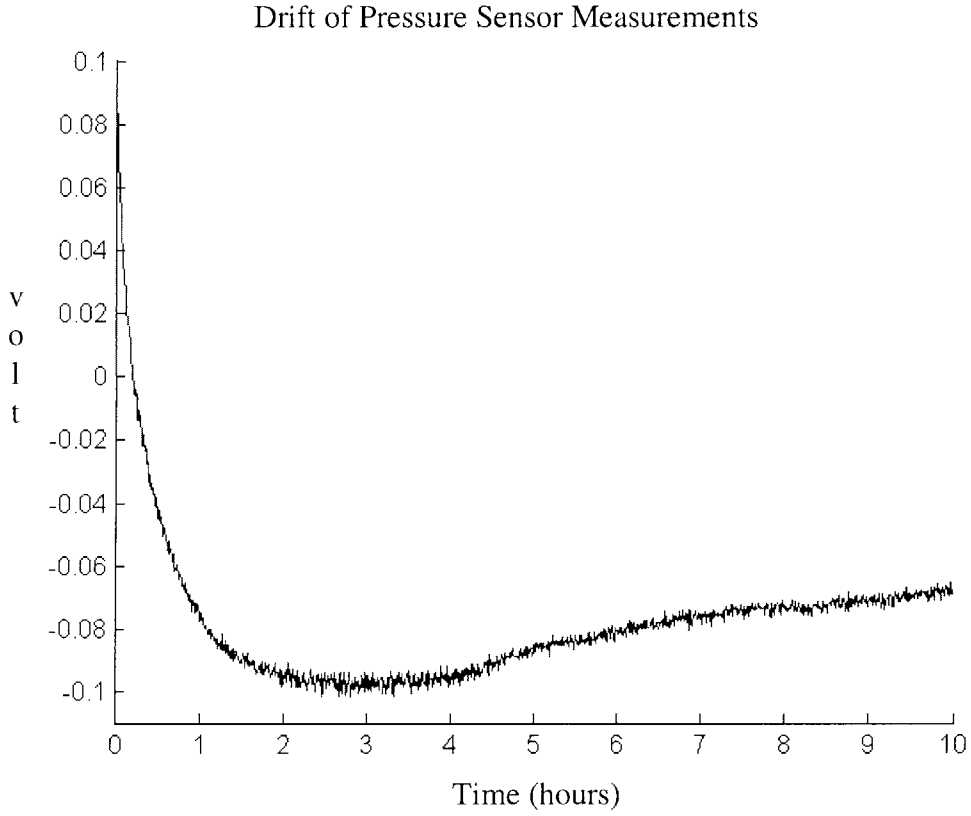

Figure 3-5. Drift of pressure sensor measurements over a 10 hour period.

We next studied the sensor to determine if the measurements of the loaded sensor changed during an experimentally relevant period of 10 minutes. In order to accomplish this, the sensor was laid flat and a stationary object was placed on top of the sensor. Data was read from each element of the sensor once a minute, for a total of 10 minutes. The measurements from each sensor element were compared over the entire time period to assess any changes in the data. We repeated the entire process using a 100 gram (Figure 3-6) and 200 gram weight.

Figure 3-7 shows the response of one row of elements after 10 trials for this given stimulus. The average standard deviation of the seven elements in the row was 0.0028146 or 0.56% of the measurement, and the average range was 0.008643 volts. This minimal change in the response of the sensor indicates the sensor's independence of time over experimentally relevant intervals (10 minutes), when loaded. The two peaks of Figure 3-7 are possibly different in magnitude because the 100 gram weight overlaid the center of one element, but not to the center of the other.

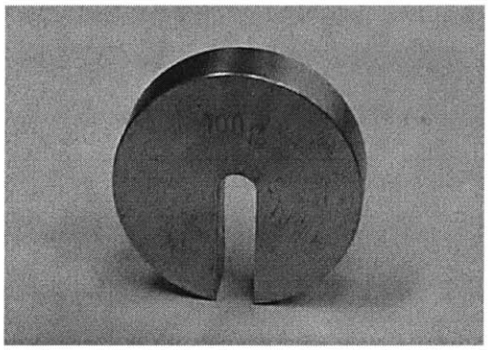

Figure 3-6. 100 gram slotted weight that was applied to sensor in the position shown.

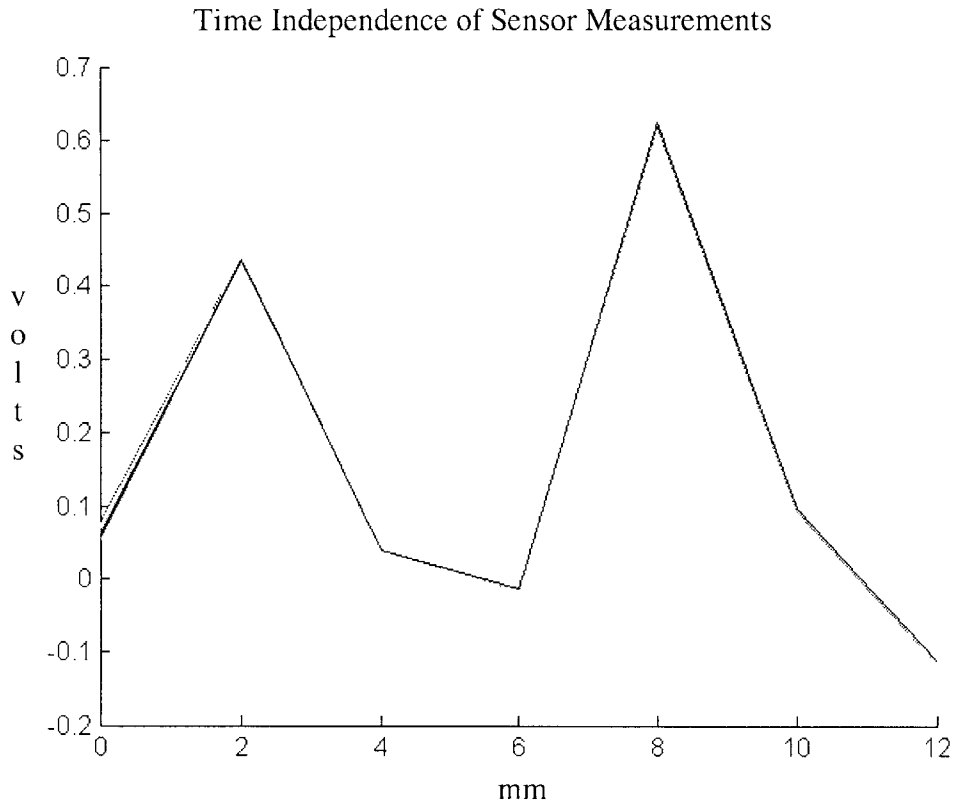

Figure 3-7. Response of one row of the pressure sensor's elements after 10 trials.

3.3.2 Repeatability

It is important to know whether the pressure sensor measurements are repeatable, and so in order to study this we laid the sensor flat and an object was placed on top of the sensor. Data was read from each element of the sensor. The object was then removed for one minute and then placed back on the sensor at approximately the same location, and data was again read from each element of the sensor. This process was repeated ten times, and the various measurements from the sensor were compared to determine if they were repeatable. We repeated the entire process using two different object curvatures and two different masses for each curvature.

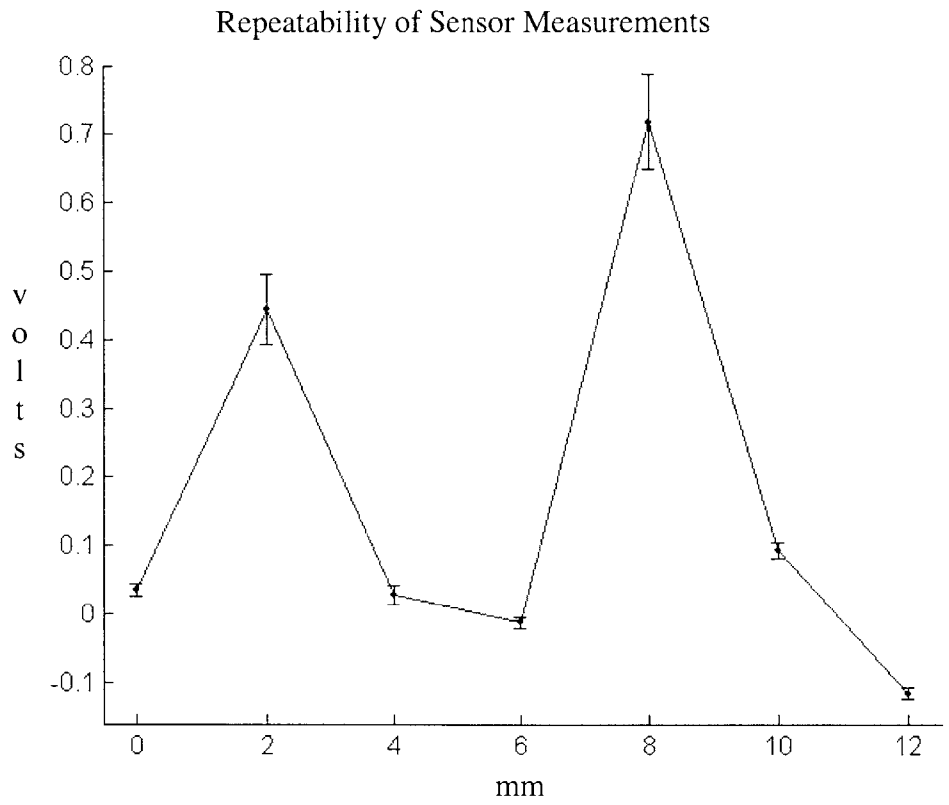

Figure 3-8. Response of the sensor to the repeated measurement of an object placed and then removed from one row of sensor elements. The thin line joins the mean measurements at different elements. The black bars indicate plus and minus one standard deviation from the mean.

Figure 3-8 shows the response of one row of sensor elements; with the line representing the average reading. The average standard deviation of the seven elements in the row was 0.02458 or 5.59% of the measurement; with an average range of 0.0686 volts. The large error present in the result is due to the object not being placed in exactly the same location when the object was removed and then replaced. The object that was applied to the sensor and the position it was applied are shown in Figure 3-6. The response of the sensor indicates that manual positioning errors can be a significant source of experimental error. Accordingly, we elected to rigidly stabilize the back of the finger pad in our experiments, and to apply the sensor with a motorized positioning stage with fine spatial precision.

3.3.3 Linearity in Response to Pressure

To further understand the characteristics of the pressure sensor, we designed a method to apply a known force along the sensor elements and record the data. The setup consisted of the motion platform, a flat plate to attach the sensor, an Aurora Scientific Model 300B Dual Mode Lever Arm System, and a stand to hold the Aurora System. The Aurora is a rotary motor with a probe at the end of lever fixed to a shaft (Figure 3-9). The motion platform was used to move the sensor in the x and y direction by finite distances, and the Aurora Lever Arm System was used to apply a known force to another object with cylindrical indenting tips of various sizes. Several different sized tips made of brass cylinders were carefully manufactured with a very flat base in order to ensure uniform contact. The diameters of the cylindrical tips that were made were 0.4mm, 0.5mm, 0.8mm, 1.2mm, 1.6mm, and 1.7mm.

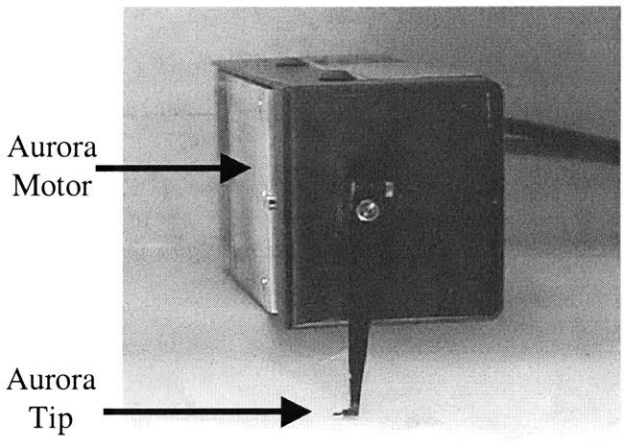

Figure 3-9. Picture of the Aurora Scientific Model 300B motor and tip.

We tested the sensor to determine if its measurements were linear with respect to force. In order to accomplish this, we applied various forces to the sensor element with the 0.5mm diameter Aurora tip. We applied nine forces each to ten points spaced at 0.2mm along the x axis of sensor element 0x54. These forces were 0.01N, 0.02N, 0.03N, 0.04N, 0.05N, 0.06N, 0.07N, 0.08N, and 0.09N. Figure 3-10 shows a plot of the sensor response to the various forces and indentation locations. Figure 3-11 shows the response at the

peak of the element which occurs approximately at 1.5mm point of Figure 3-10. A linear fit to the data had a slope of 0.1726 volt/gram, a bias of -0.1830 volt, and a R^2 value of 0.9778. Figure 3-12 shows the response of the element at the 1.0mm point of Figure 3-10. A linear fit to these measurements had a slope of 0.1269 volt/gram, a bias of -0.1008 volt, and a R^2 value of 0.9846. In both cases, the sensor output with increasing force was slightly sigmoidal. Over the force ranges shown in Figures 3-11 and 3-12 deviation from linearity was found to be 6.5% to 7.1% of the maximum reading.

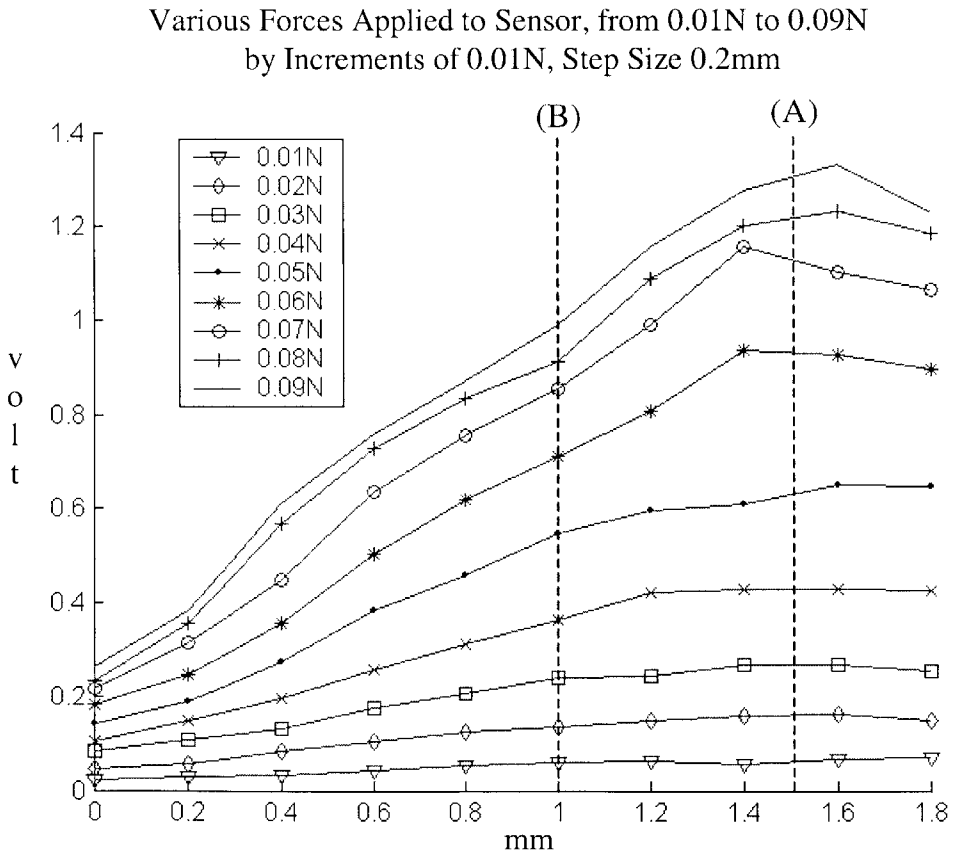

Figure 3-10. Various forces of 0.01N to 0.09N were applied to element 0x54 with a 0.5mm diameter cylindrical tip. The center of the element denoted (A) and 0.5mm to the left of the center of the element (B) are marked by dashed lines.

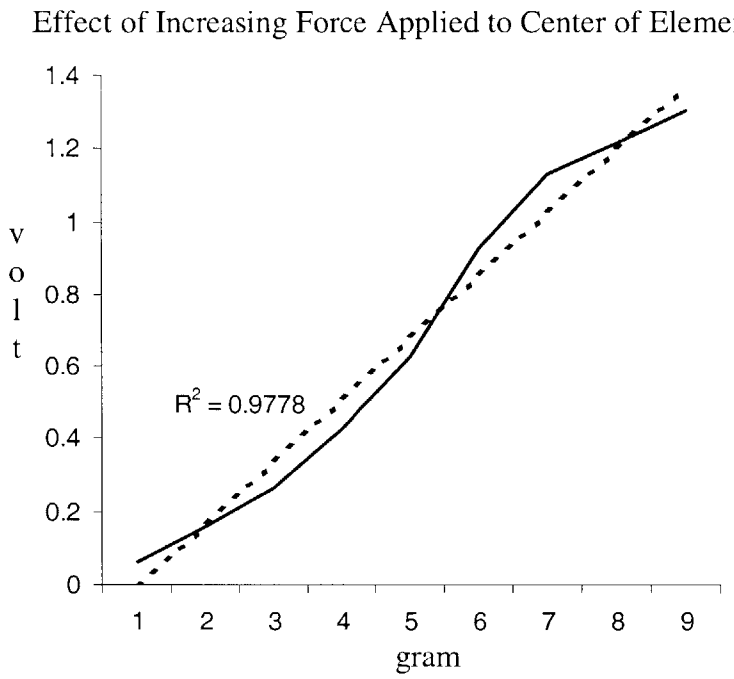

Figure 3-11. Various force levels applied to the center of element 0x54 (dashed line in Figure 3-10 (A)).

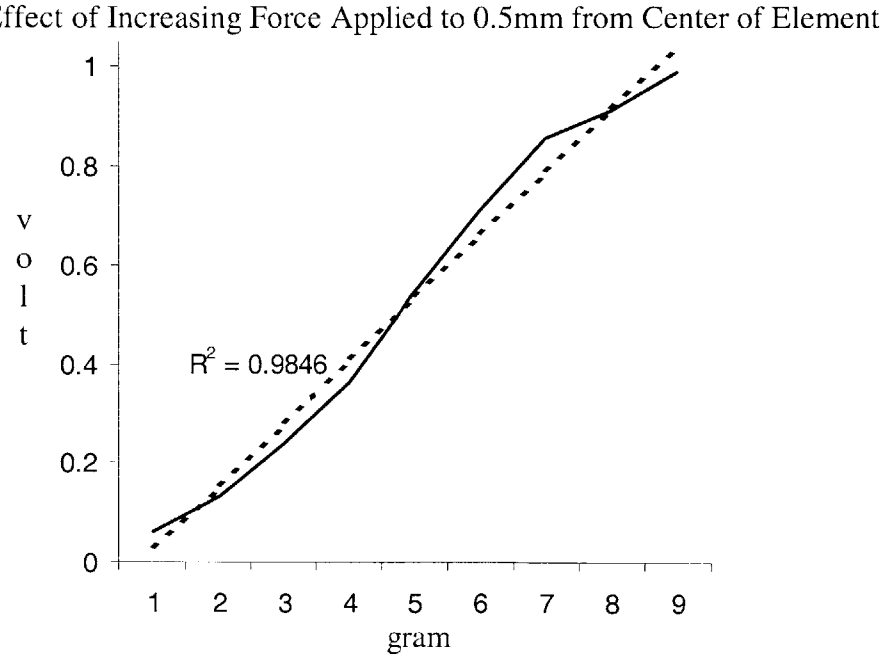

Figure 3-12. Various force levels applied to 0.5mm to the left of the center of element 0x54 (dashed line in Figure 3-10 (B)).

We also tested the sensor to see if applying different sized indentor tips to an element with the same force would cause an appropriate scaling of the response. We applied the same 0.075N force using the Aurora 0.4mm, 0.8mm, 1.2mm, and 1.6mm tips to element 0x54, and we found that the peak values were approximately linear, as a function of tip diameter. Figure 3-13 shows the result.

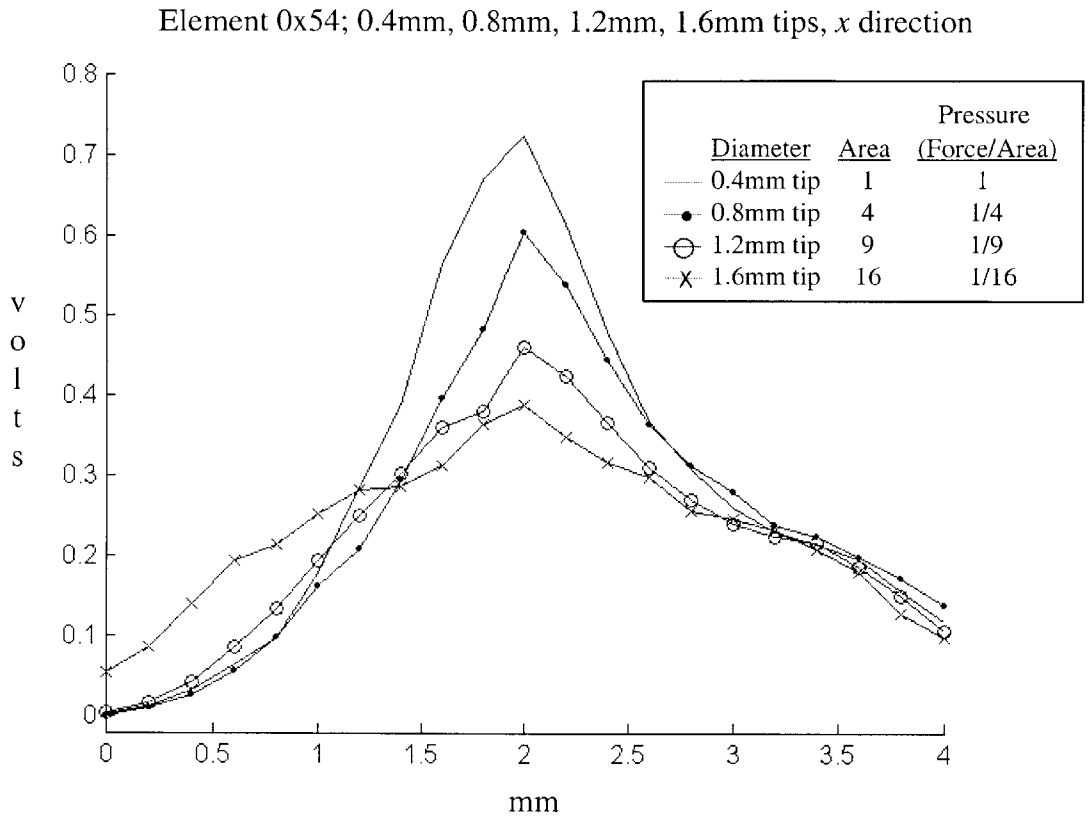

Figure 3-13. The same force applied to element 0x54 along the positive x direction using the Aurora 0.4mm, 0.8mm, 1.2mm, and 1.6mm tips.

3.3.4 Anisotropy

The response profile of the sensor was different when the indentor was stepped in the x direction than in the y direction. To explore this anisotropy, we attached the sensor to the flat plate with double sided tape in the orientation shown in Figure 3-3a. We applied a force of 0.075N with the 0.5mm Aurora tip to element 0x56 and stepped along the x

direction. We then returned to the center of element 0x56 and applied a force of 0.075N while stepping along the y direction. Figure 3-14 shows both of these results. The response of the element has a narrow distribution when the indentor is applied along the x direction, and the response in the y direction is broader.

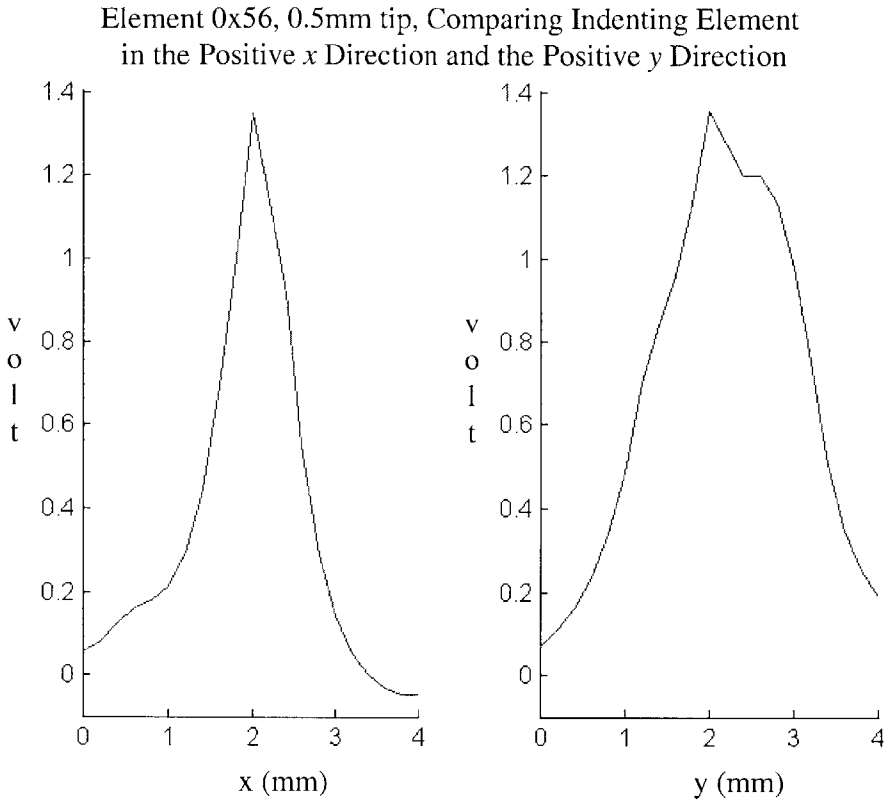

Figure 3-14. Aurora tip with 0.5mm diameter translated along the positive x and y direction of element 0x56. The response of the element has a narrower distribution when the indentor is applied along the x direction than in the y direction.

This result implies that the direction in which measurements are read from the sensor is important. To further confirm the anisotropy and determine any effects of loading sequence, we rotated the orientation of the sensor on the flat plate 90° degrees, as shown in Figure 3-15. We then repeated the previous test by stepping along the x direction, returned to the center of element 0x56, and then stepped along the y direction. Figure 3-16 shows both of these results where x_1 is analogous to y (but increases in the opposite direction) in Figure 3-13 and y_1 is identical to x in Figure 3-14. From these results, we

can conclude that the sequence of loading does not have an effect, but the orientation of the sensor when taking measurements does matter.

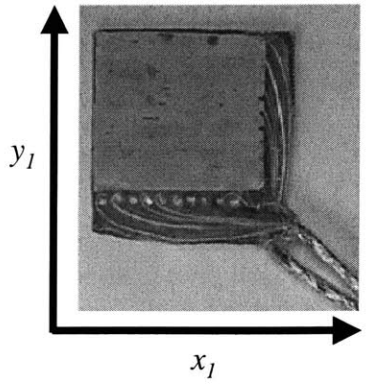

Figure 3-15. Pressure sensor rotated 90° degrees. The new coordinate system consisting of the positive x_1 and y_1 directions are specified.

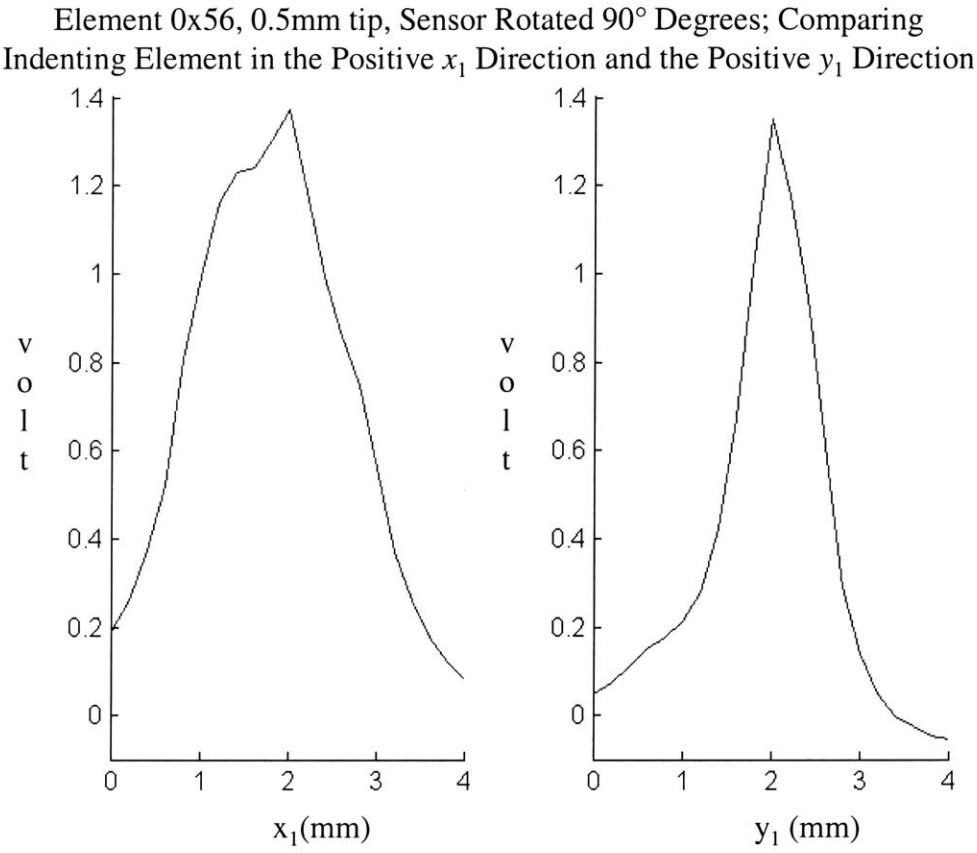

Figure 3-16. Aurora tip with 0.5mm diameter translated along the new positive x_1 and y_1 direction of element 0x56.

3.3.5 Inter-Element Variability

We next studied the similarities and differences between different elements in the sensor array. We tested the sensor to see if other elements exhibited a narrower response in the *x* direction than the *y* direction. We did this by applying the same amount of force from the 0.5mm Aurora tip across elements 0x54 and 0x56. We first applied a force of 0.075N to each element and stepped along the *x* direction, and then returned to the center of each element and applied the same force while stepping along the *y* direction. Figure 3-17 show the results of a) element 0x54 and b) element 0x56. The response along the *x* was narrower than the response in the *y* direction for both elements. The coordinate system used is the same as shown in Figure 3-3a.

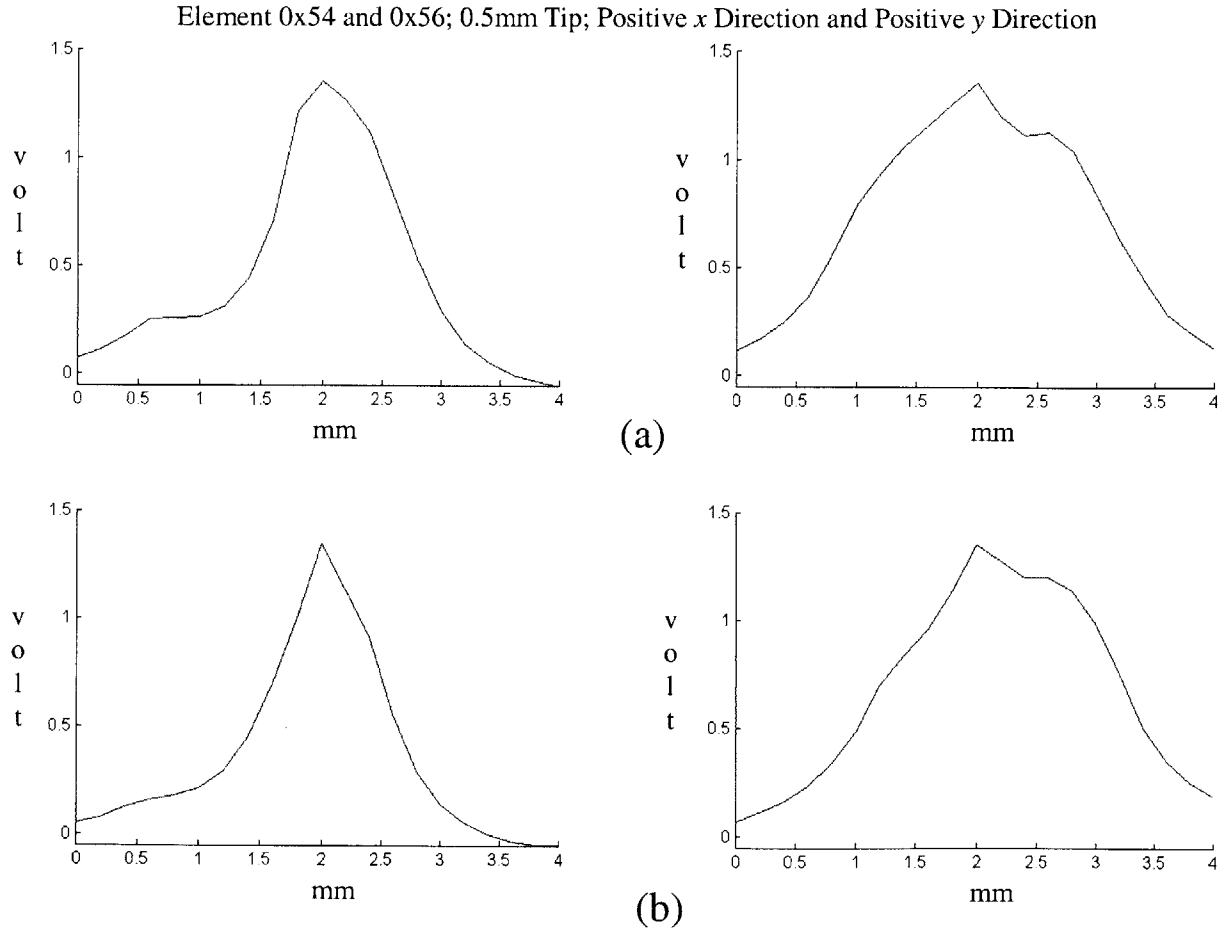

Figure 3-17. The same 0.075N force from the 0.5mm Aurora tip was applied in the positive *x* and *y* direction for a) element 0x54 and b) element 0x56.

We also tested various elements to determine if their peak values and response were the same. We applied the same 0.075N force along the *x* direction, using the Aurora 0.4mm, 0.8mm, 1.2mm, and 1.6mm tips, to four different elements. The elements we used were elements 0x52, 0x54, 0x63, 0x65. Figure 3-18 shows the results from the four elements. We found that all four elements had a similarly shaped response. However, the peak value of each element was different. Elements 0x52 and 0x65 had similar peak values, while elements 0x63 and 0x54 had similar peak values. No two elements had the exact same peak value even though the same force was applied to each sensor.

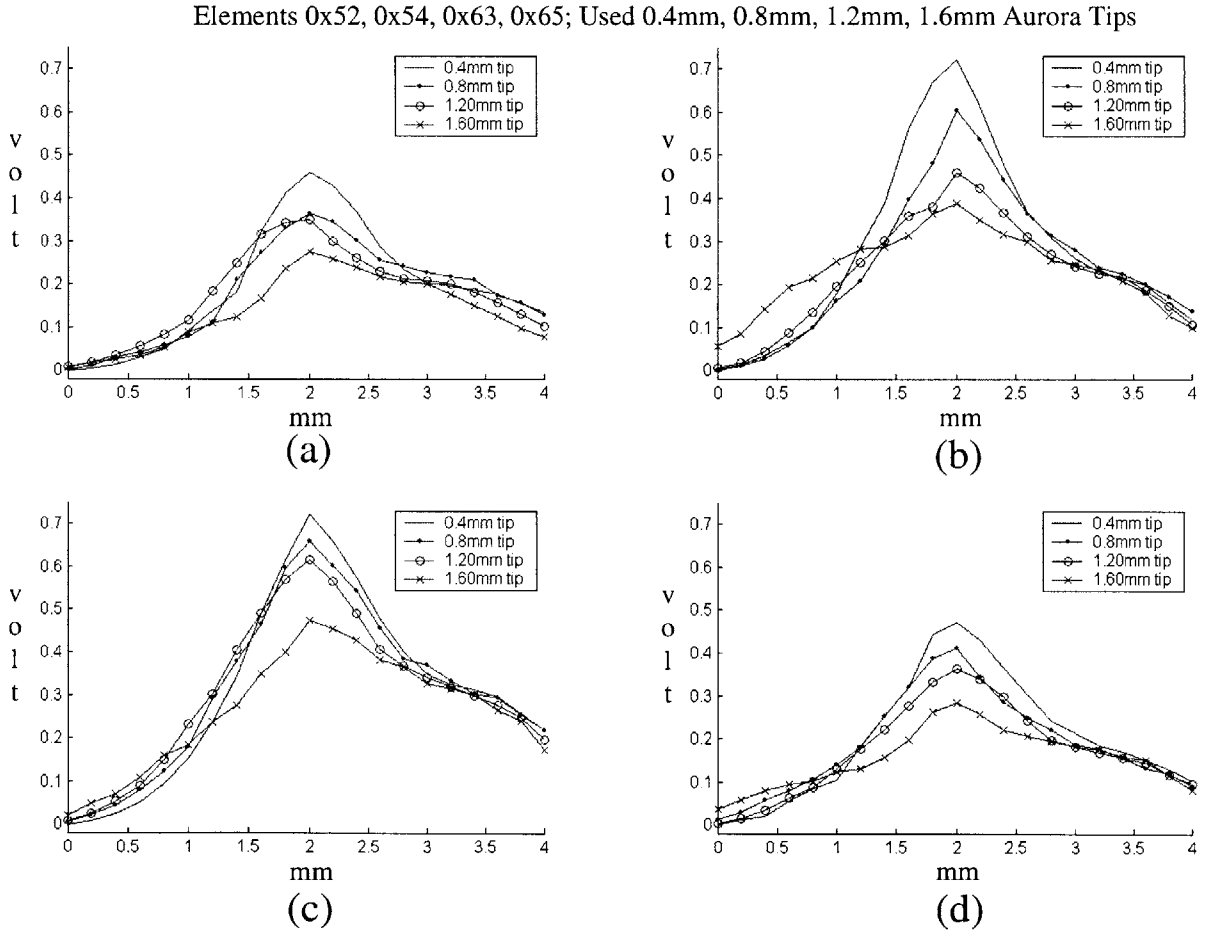

Figure 3-18. A force of 0.075N force using the Aurora 0.4mm, 0.8mm, 1.2mm, and 1.6mm tips were applied to elements a) 0x52, b) 0x54, c) 0x63, and d) 0x65. All measurements were taken in the *x* direction.

3.3.6 Spatial Response Profile

We were interested in measuring the response of an element to a line load, because the spatial response profile (response of the sensor plotted as a function of the spatial position of the load) would aid us in using signal processing techniques to increase the spatial resolution of pressure measurements. In order to measure the spatial response profile we placed the sensor around the 1 inch diameter cylinder. We slightly dulled a razor blade to protect the sensor, and then placed it in a vice to hold it so that measurements were taken along the x direction of the sensor. The thickness of the razor edge was measured to be 0.0023 inches (0.05842mm) using a Nikon Measurescope. Figure 3-19 shows the experimental setup. Data from only element 0x54 was accessed during this experiment.

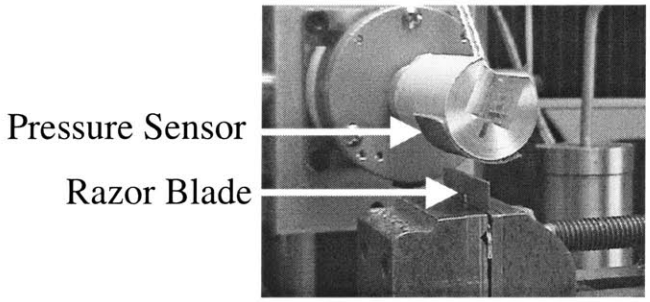

Figure 3-19. The experimental setup used to measure the spatial response profile of element 0x54 of the pressure sensor. A dulled razor blade is used to indent the sensor while it is wrapped around a 1 inch diameter cylinder.

We lowered the sensor onto the razor blade, with a small amount of force. Then we raised the sensor and moved it in the x direction by a distance of 0.033mm, and again applied the load to the razor blade. We repeated this process until we translated the razor across the one element, and then repeated this entire process twice. The first time we applied a load of 86.3mN to the razor blade which produced a pressure of 52,965 Pascals under the razor blade. The second time we applied a load of 183.4mN to the razor blade which produced a pressure of 112,520 Pascals under the razor blade. Figure 3-20 shows the results of applying the line load to the sensor both times along the x direction.

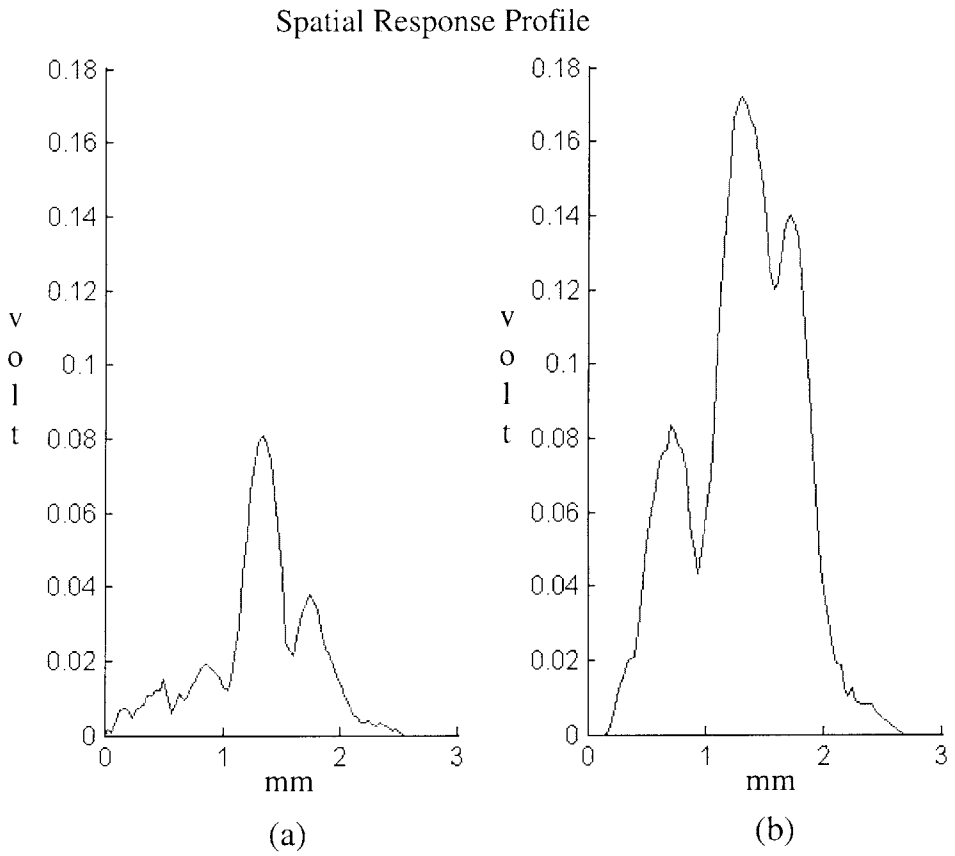

Figure 3-20. Spatial response profile produced by a razor blade indenting the sensor element 0x54 with a net force of 86.3mN and 183.4mN, respectively. Both measurements were taken along the *x* direction of the sensor (refer to Figure 3-3a).

3.3.7 Sensor Resolution

The size of each element of the sensor is 2mm by 2mm, but given the non-uniformity of the response to loads across its surface, we wanted to determine the smallest possible spatial resolution of the sensor response. We accomplished this by having a pattern of lines micro-machined on a silicon wafer and then measured the sensor response to this pattern. Figure 3-21 shows the pattern we micro-machined onto a silicon wafer using photolithography. The height of each line is 0.10mm and the thickness of each line is 0.021mm.

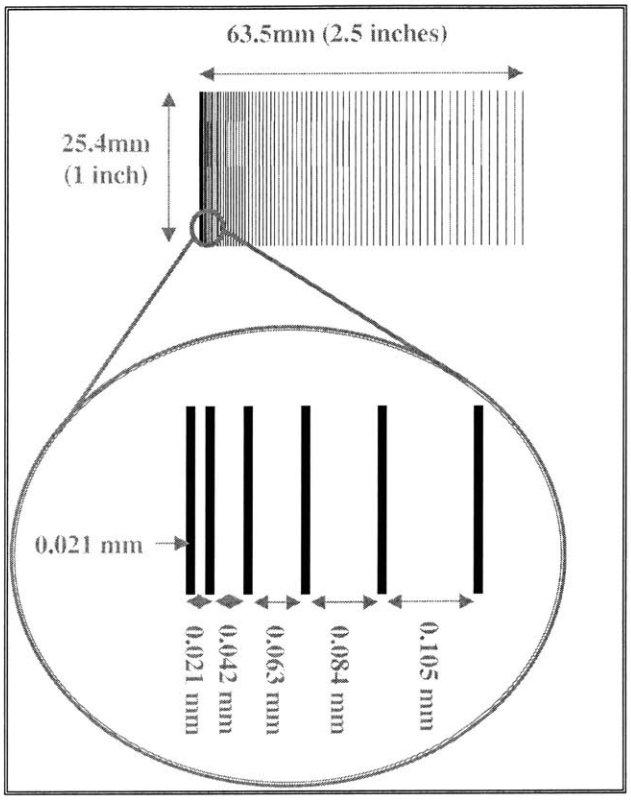

Figure 3-21. Pattern micro-machined onto a silicon wafer using photolithography. The height of each line is 0.10mm and the thickness of each line is 0.021mm.

In order to measure the response of the sensor to the silicon wafer, we first placed the sensor around the 1 inch diameter cylinder, and then applied the sensor to the wafer with a small amount of force, read data from one sensor element, removed the sensor from the wafer, and then moved the sensor by a finite distance along the x direction of the wafer. We repeated this process until we translated it across the entire wafer (Fig. 3-22). Figure 3-23 shows the response of the sensor to the silicon wafer split into smaller sections for easier viewing.

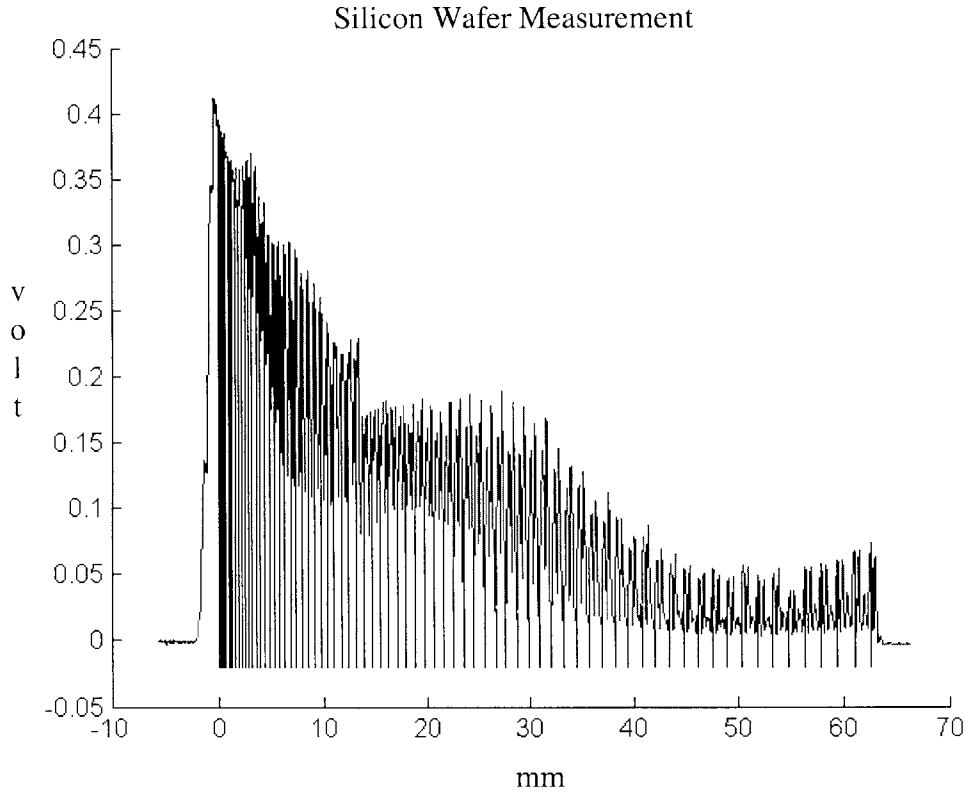

Figure 3-22. Response of the sensor to different positions across the silicon wafer. The vertical lines in the picture correspond to the location of the bars in the silicon wafer.

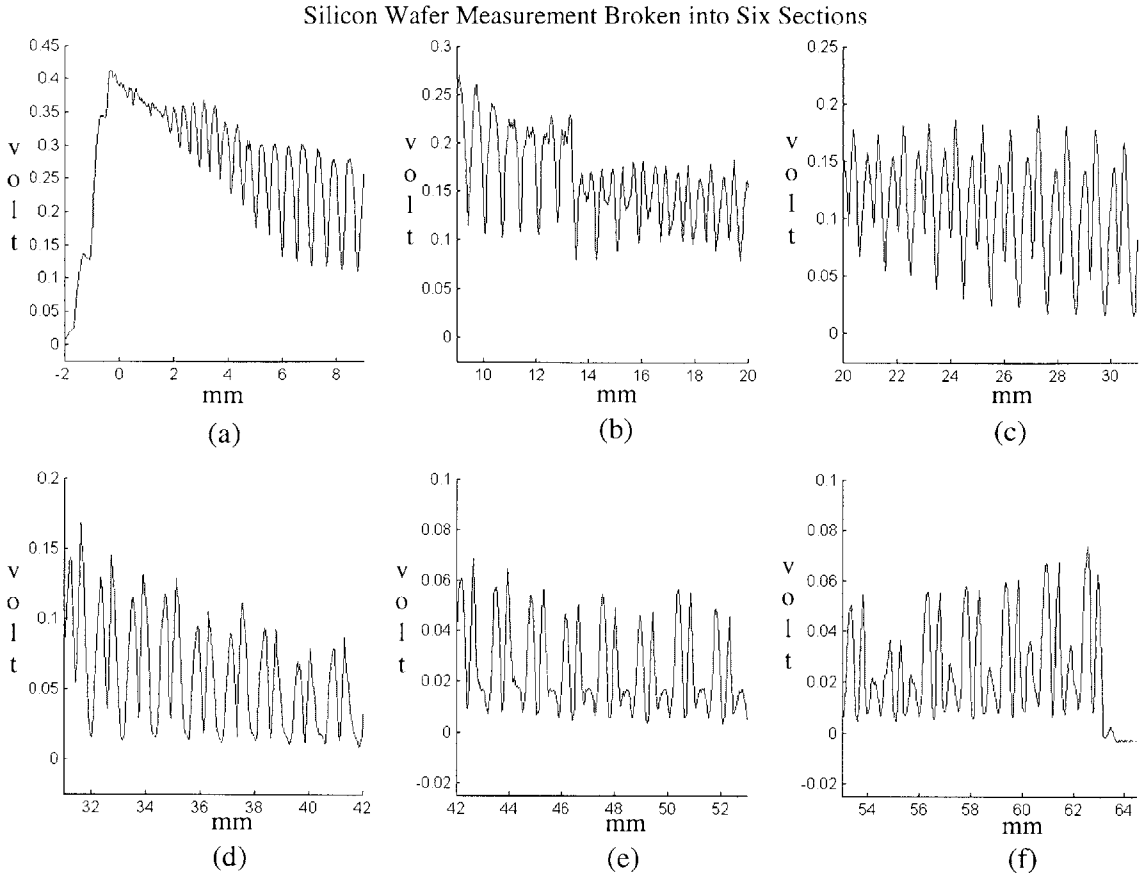

Figure 3-23. Response of the sensor to silicon wafer shown in Figure 3-21. The response is split into 6 separate sections; a) 0mm to 9mm, b) 9mm to 20mm, c) 20mm to 31mm, d) 31mm to 42mm, e) 42mm to 53mm, and f) 53mm to 64mm.

The resolution of the sensor can then be determined by measuring where two neighboring bars can be clearly distinguished from the sensor response. We used the Rayleigh's criterion to justify the finest resolution possible for the sensor. Rayleigh's criterion states that two similar images can just be resolved when the first minimum of one image falls on the central maximum of the other image [Serway, 1990]. Figure 3-24 shows the spatial profile response of the sensor at a point where it is just resolvable. The spatial resolution based on Rayleigh's criterion is 1.0mm.

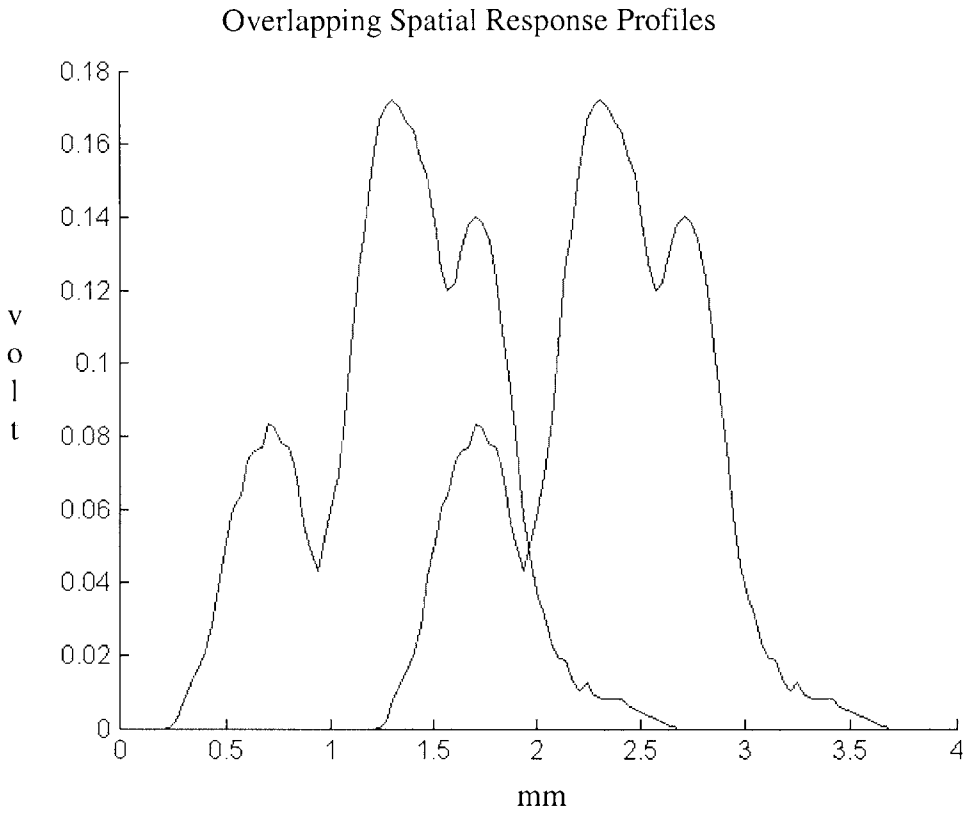

Figure 3-24. Overlapping spatial response profile. The point at which the two images are resolvable occurs when the first minimum of one image falls on the central maximum of the other image. A distance of 1.0mm separates the central peaks.

3.4 Pressure Sensor Calibration

The output of the pressure sensor to the PC is in volts, and so in order to convert the pressure sensor output of voltage to pressure, we needed to calibrate the sensor. To do this we applied a uniform pressure over the surface of each element using water pressure, placing the sensor on a flat surface and a waterproof bag on top of the sensor. The bag was filled with water to various heights ranging from 3.6 inches to 7.6 inches and readings were taken from all elements of the pressure sensor. The entire sensor was completely covered by the bag of water to avoid stress concentrations along the edges of the sensor array during calibration .

The pressure was then calculated from the height of the water using the equation, $\Delta p = \rho g h$, where ρ is the density of water, g is gravity, and h is the height of the water in the bag. Figure 3-25 shows the pressure from all elements. The voltage from each element can be converted to pressure by fitting a line to the data and using it as a voltage to pressure conversion table. Figure 3-26 shows the data from element 0x54. A linear line was fit to the data and found to have a slope of 0.00002288 volt/gram, and a R^2 value of 0.962.

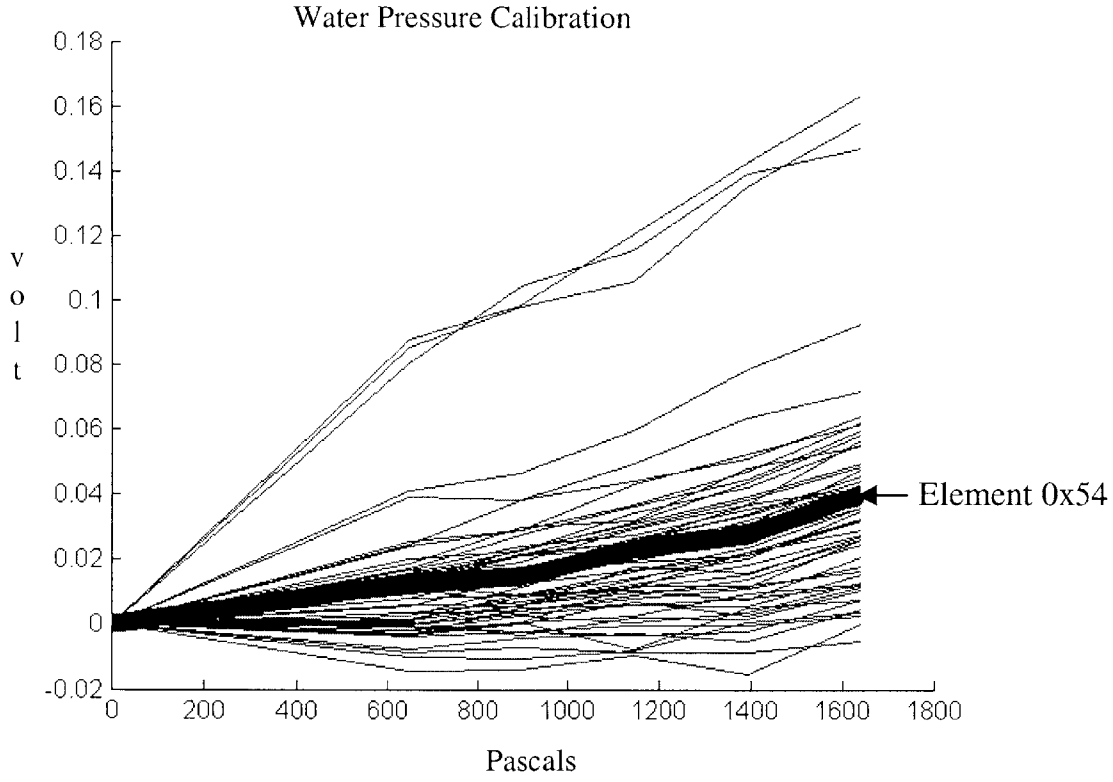

Figure 3-25. Various levels of water pressure applied to all elements of the sensor in order to convert from sensor voltage to pressure.

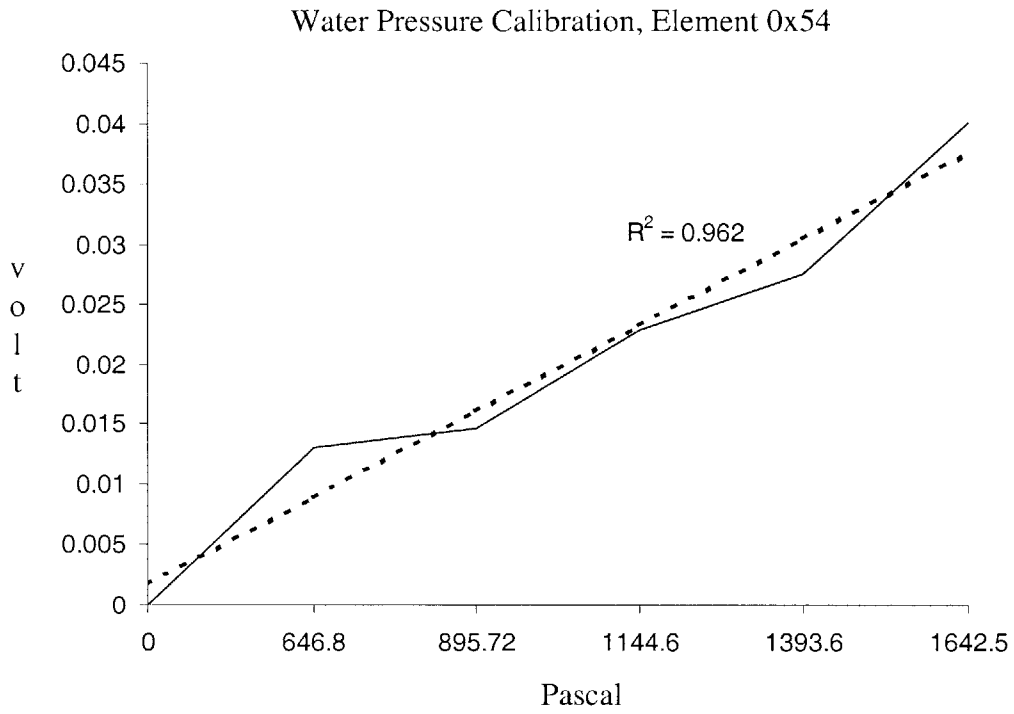

Figure 3-26. Water pressure calibration of element 0x54. A linear fit to the data had a slope of 0.00002288 Volt/Pascal, and a R^2 value of 0.962.

3.5 Linearity in Terms of Spatial Summation

The response of a sensor element to a line load was described in Section 3.3.6, and the response of each element of the sensor to a uniform load was described in Section 3.4. We want to determine whether the sensor elements exhibit linearity in terms of spatial summation. In other words, we wanted to see if the sensor response to uniform pressure could be predicted by appropriate responses to the line load. Figure 3-27 illustrates this question of whether the response of the sensor to uniform water pressure over the entire element is equal to the summation of the response of the sensor to a line load across the element.

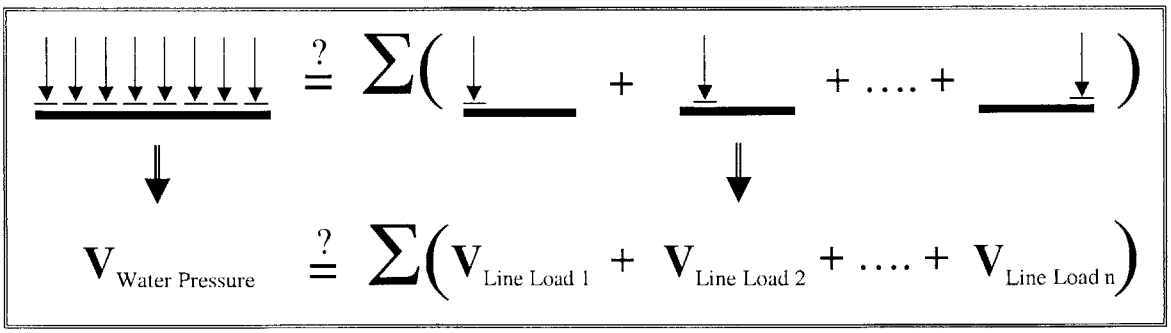

Figure 3-27. Illustration of whether the response of the pressure sensor to uniform water pressure is equal to the summation of the responses of the sensor to a different location of the line load. The uniform water pressure over one sensor element is illustrated on left side of the equal sign. The summation of the response from a line load translated across one sensor element is illustrated on the right of the equal sign.

The pressure under the razor blade, used to measure the spatial response profile of element 0x54, was 52,965 Pascals when a load of 86.3mN was applied to the sensor, and 112,520 Pascals when a load of 183.4mN was applied to the sensor. We did not measure the response of the sensor to such a large uniform pressure in our water pressure calibration; rather we extrapolated from the curve in Figure 3-26 to determine what voltage we would expect. We discretely sampled both of the voltage distributions in Figure 3-20 with 41 points, corresponding to 41 widths of the razor blade. We then summed those 41 voltages.

The summation of the line load across element 0x54 shown in Figure 3-20b was found to equal 2.5834 volts, while under the same load the voltage from a uniform load was found to equal 2.9785 volts. This result indicates that the pressure sensor exhibits approximate linearity in terms of spatial summation for loads over 0.15N, since the two summations differ by roughly 13%. The summation of the line load across element 0x54 shown in Figure 3-20a was found to equal 0.7703 volts, while under the same load the voltage from a uniform load was found to equal 1.4003 volts. This result indicates that the pressure sensor does not exhibit linearity in terms of spatial summation under small loads, since the two summations differ by roughly 45%. This difference may have been caused by experimental error within the water pressure calibration method, or may have been due to non-linearity in spatial summation by the sensor. Repeated calibration using

water pressure would be required to put an upper bound on the contribution of this calibration method to the observed percent difference.

3.6 Prospects for Deconvolution

Simulation suggests that deconvolution may increase the spatial resolution of the pressure measurements. Figure 3-28 shows simulated, noise-free pressure data before (left) and after (right) deconvolution. The deconvolved pressure distribution shows an increased resolution of finger ridges and grooves. However, in order for deconvolution to improve the spatial resolution of pressure measurements, the pressure sensor must produce linear measurements and be shift-invariant.

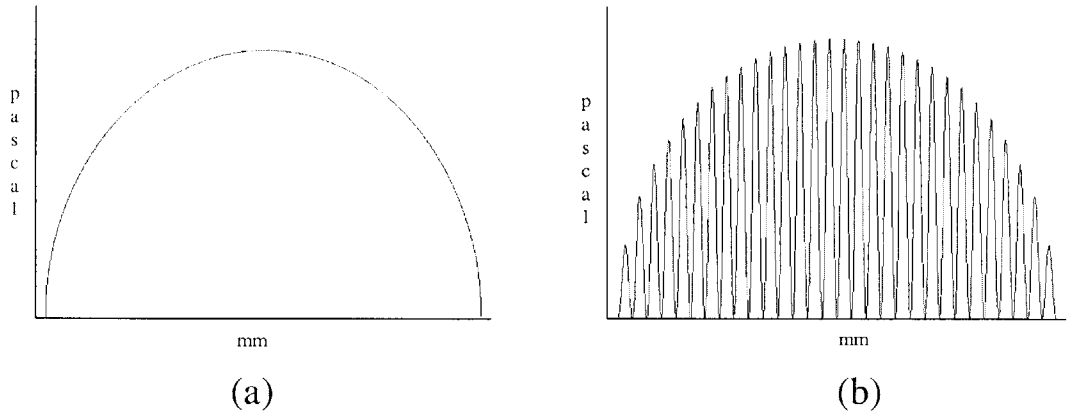

Figure 3-28. Schematic illustrating the pressure distribution measurements a) before the use of deconvolution and b) after the use of deconvolution. The use of deconvolution will increase the spatial resolution of the measurements in order to determine the pressure over finger ridges and grooves more clearly.

The spatial response properties of the sensor measured in section 3.3 which shows that the sensor response varies with respect to load location, indicates that the use of deconvolution might lead to finer reductions. However, we observed many sources of noise that might limit the success of this technique. Sensor noise gave repeated measurements of the same load a standard deviation of 0.55%. When forces of 0.01-

0.09N were applied, non-linearity in response to the increasing forces lead to errors in pressure that were 0 to 7.1% of the voltage observed at 0.09N. Non-linearity in terms of spatial summation was shown to distort the measurement by 13% for loads over 0.15N and by as much as 45% for loads under 0.15N. Finally, the spatial response profile (Figure 3-20) of the sensor had several peaks. These observations suggest that deconvolution – which is sensitive to all of these sources of error – may be difficult.

3.7 Summary

In this chapter we established to what extent sensor measurements were repeatable, linear, and anisotropic. Gain for each element of the sensor was found to vary significantly. The spatial response profile was measured and the sensor was measured using a line load. A uniform load under water pressure was used to find a factor for converting sensor voltages to pressures. Due to the anisotropy of the sensor, we chose to shift the sensor in the x direction exclusively. We also examined the use of deconvolution to increase the spatial resolution of pressure measurements.

4.0 Finger Pad Pressure Measurement

4.1 Methods

We measured the pressure distribution on the index finger pads of five subjects, as two rigid indentors were used to load the pad at forces ranging from 0.24N to 1.75N. The indentors were cylindrical, with diameters of 1 and ½ inch. The pressure sensor array, which was situated between the indentor and skin, was used to sample interfacial pressure at different points in the contact area. Figure 4-1 shows orientation of the finger and cylinder, and our convention for displaying the interfacial pressure in subsequent figures.

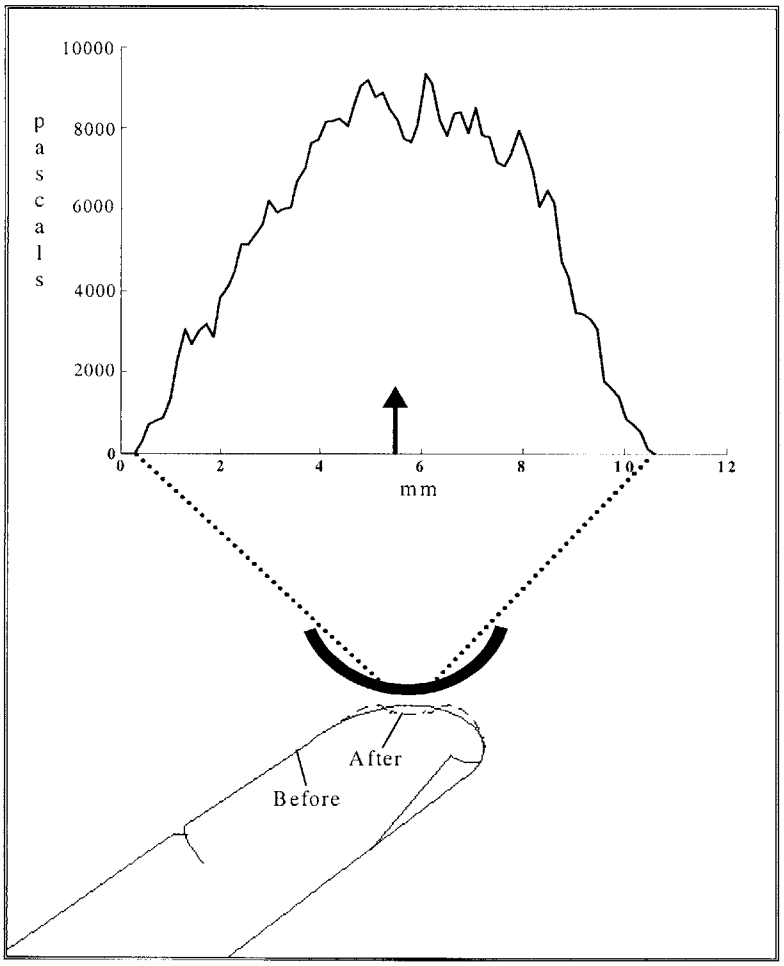

Figure 4-1. Illustration of the measurement of the pressure distribution from the finger pad using a curved indentor. The deformation of the finger before and after a load is applied are marked. The arrow indicate the force or pressure components measured.

During the experiment we measured voltage on one element (0x54) of the pressure sensor array. At the start of each measurement, we used the motion platform to rotate the indentor and pressure sensor to a known position on the fingertip and then applied a known net force. Between measurements, the motion platform raised the indentor off the fingertip, and then rotated it by a small known arc length. The sensor was then returned to the fingertip with the same net force, and another pressure measurement was taken. This process was repeated until the sensor element had rotated entirely across the fingertip contact region. All measurements were saved in a PC data file. Figure 4-2 illustrates the process. To obtain fine spatial resolution the shifts in sensor location were far smaller than the 2mm sensor element width. In a typical experiment, 100 measurements were taken over a 10mm arc. To minimize the effect of drift in the sensor, the data just before contact during each indentation was used as a baseline for pressure measurements.

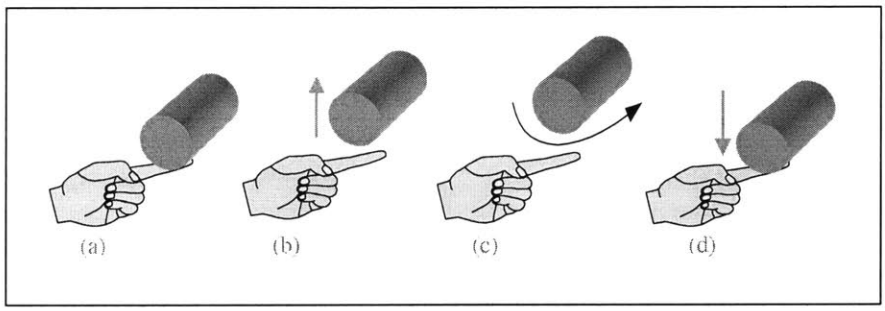

Figure 4-2. The process used to measure the pressure distribution of the finger pad. The pressure sensor is situated between the object and finger pad. The finger pad (a) is indented with the cylindrical object, (b) the object is removed from the finger pad, (c) the object is rotated by a known amount, and then (d) the object again indents the finger pad. This process is repeated until the pressure sensor scans the entire contact area of the finger pad.

4.2 Results

We applied various net forces with two different cylindrical indentors to the finger pads of five subjects. Our results show the effect of changes in net force and indentor curvature on the magnitude and shape of the pressure distribution. Asymmetry in the

pressure distributions was expected, since the resting curvature of the finger pad surface varied from the proximal to distal edge of the contact area.

4.2.1 Inter-Subject Variability

We first consider the effect of indenting the finger pad of various subjects with the same sized cylinder. Figure 4-3 compares the results of applying a 0.5N net force with a 1 inch diameter cylinder to the finger pad of subjects 1 and 2. The resulting magnitude and shape of the surface tractions are very similar for both subjects.

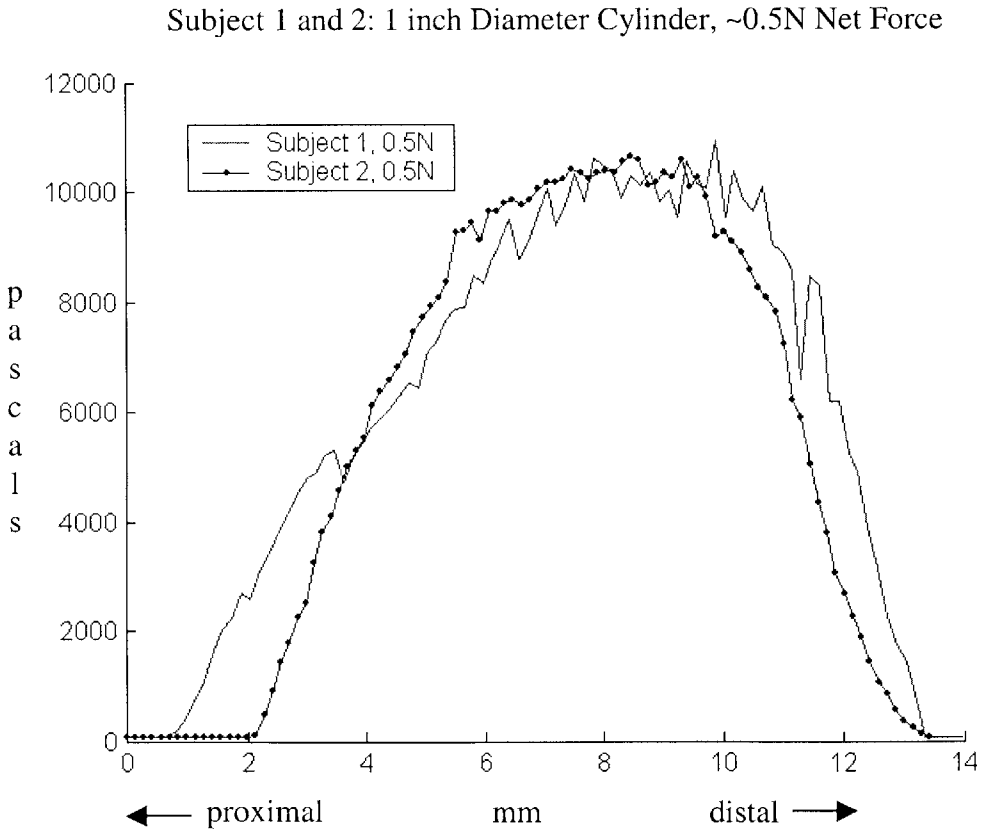

Figure 4-3. Pressure distribution measurement of subject 1 and subject 2. Both subjects were indented with net force of 0.5N using a 1 inch diameter cylinder.

Figure 4-4 compares the results of applying approximately a 0.25N net force with the ½ inch diameter cylinder to the finger pad of subjects 2, 3 and 4. The shape of the surface tractions are very similar for all three subjects. The peak values of the surface tractions vary between the subjects by about 50%. This difference may in part reflect noise in the load cell sensing net force, since 0.25N is in the bottom 2.5% of the operating range of the device.

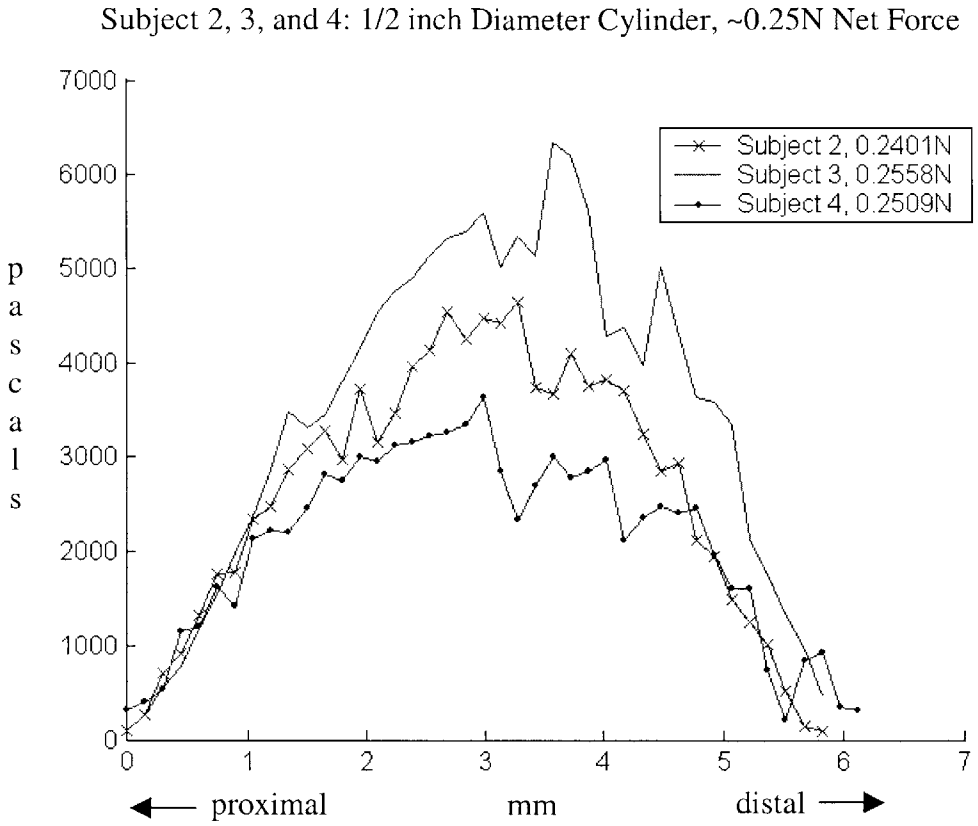

Figure 4-4. Pressure distribution measurement of subjects 2, 3, and 4. All three subjects were indented with a net force of approximately 0.25N using a ½ inch diameter cylinder.

4.2.2 Effect of Varying Radius

Figure 4-5 compares the results of applying a net force of approximately 0.5N with both the 1 inch and ½ inch diameter cylinder to the finger pad of subject 5. Both surface tractions have an approximately trapezoidal distribution. As expected, the peak

magnitude of the surface traction under the ½ inch diameter cylinder is greater than the peak magnitude under the 1 inch diameter cylinder. Accordingly, the lower peak pressure under the 1 inch diameter indentor is compensated by the greater width.

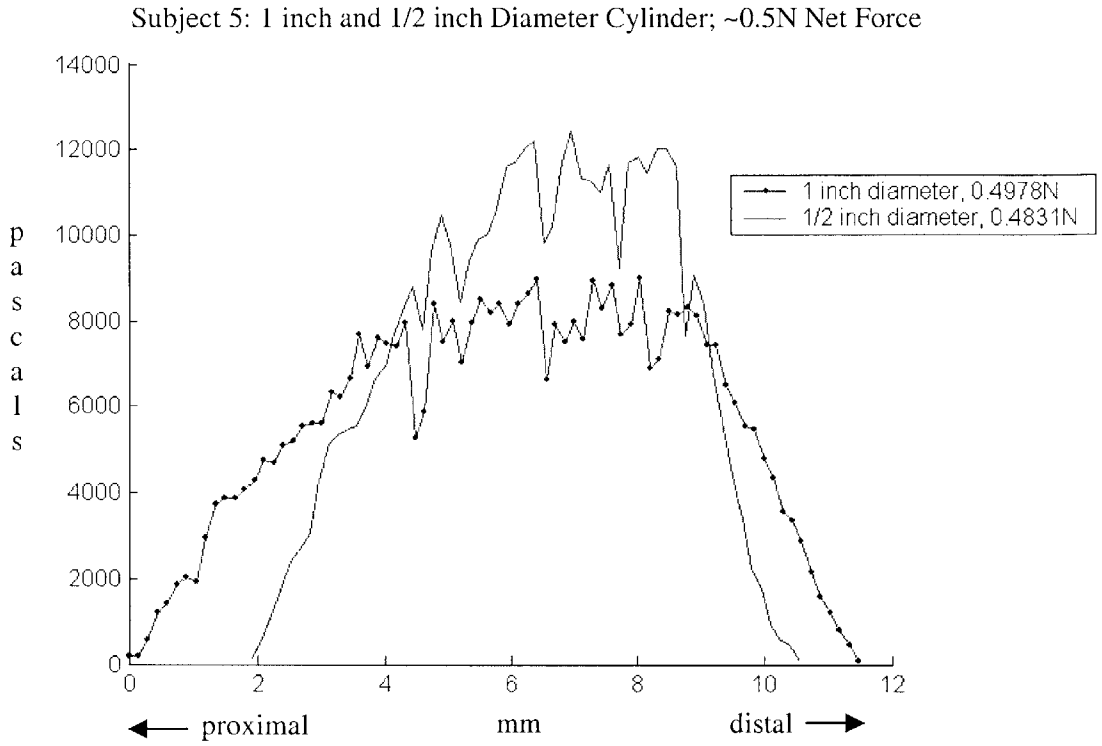

Figure 4-5. Pressure distribution measurement of subject 5 using a 1 inch diameter cylinder with a net force of 0.4978N compared to the pressure distribution measurement of subject 5 using a ½ inch diameter cylinder with a net force of 0.4831N.

4.2.3 Varying Net Force

We varied the net force that was applied to the finger pad of the subjects while using the same sized cylindrical indentor. Figure 4-6 shows the results of applying a net force of 0.2215N, 0.5116N and 1.0398N to the finger pad of subject 2 with the same 1 inch diameter cylindrical indentor. The general shape of the pressure distribution for all three force levels is similar, with the magnitude of the pressure distribution increasing as the net force level increases. The width of the surface traction also increases as the net force increases, though this effect appears to saturate between 0.5N and 1.0N grams.

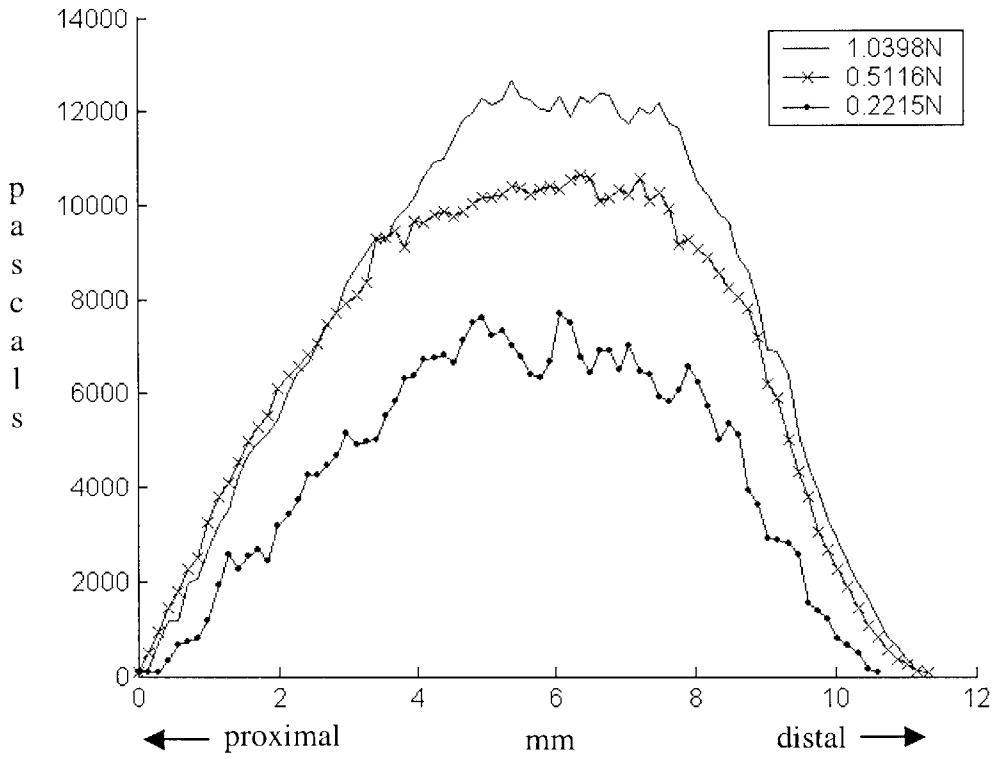

Figure 4-6. Pressure distribution measurement of subject 2 using a 1 inch diameter cylinder with a net force of 0.2215N, 0.5116N and 1.0398N.

Figure 4-7 shows the results of applying a net force of approximately 0.50N, 1.0N, and 1.75N to the finger pad of subject 1 with the same 1 inch diameter cylindrical indentor. Once again, the general shape of the pressure distribution for all three force levels is similar. The magnitude and width of the pressure distribution increases as the net force level increases.

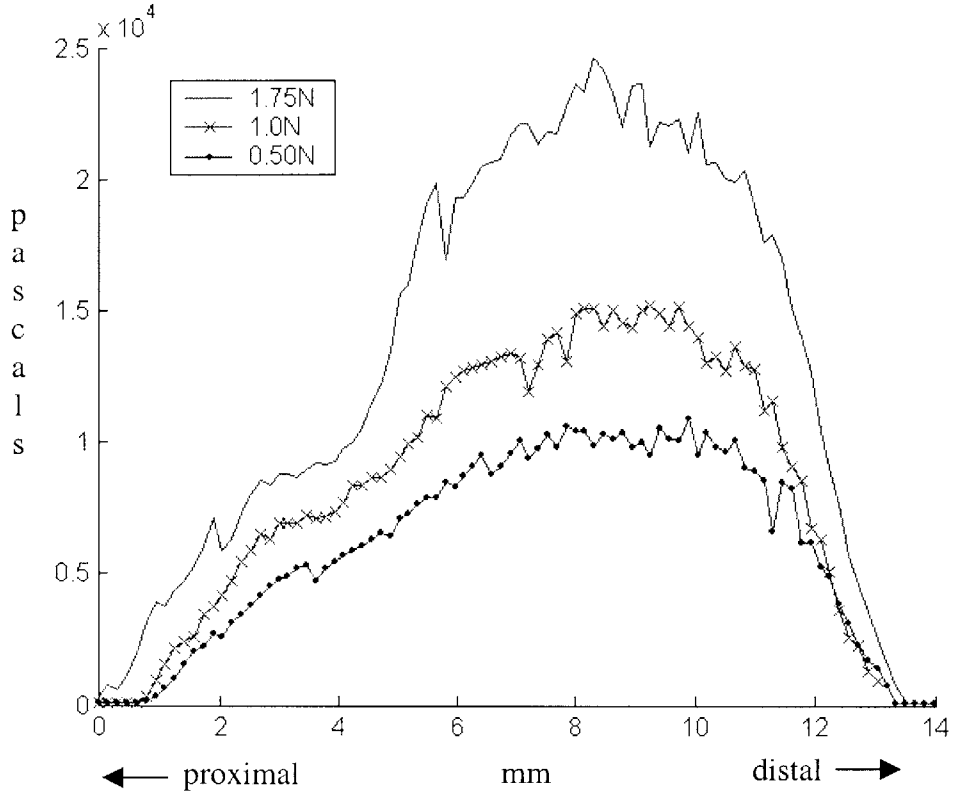

Figure 4-7. Pressure distribution measurement of subject 1 using a 1 inch cylinder with a load of 0.50N, 1.0N, and 1.75N.

Figure 4-8 shows the results of applying a net force of 0.2401N, and 0.5027N to the finger pad of subject 2 with the same ½ inch diameter cylindrical indentor. The general shape of the pressure distribution for both force levels is similar. The magnitude and width of the pressure distribution increases as the net force level increases.

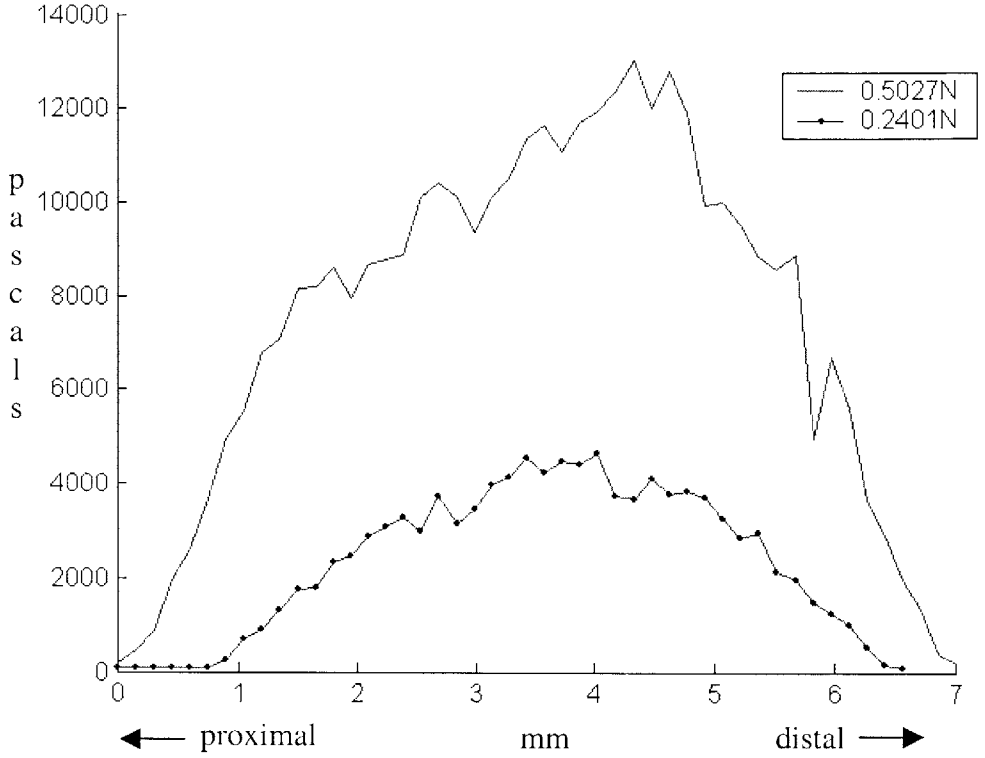

Figure 4-8. Pressure distribution measurement of subject 2 using a ½ inch diameter cylinder with a net force of 0.2401N and 0.5027N.

4.2.4 Finger Ridges

We were interested in the effects of varying the step size between samples. Figure 4-9 shows the results of applying a net force of approximately 1.50N to the finger pad of subject 1 with the 1 inch diameter cylindrical indentor for two different sample sizes. The samples were taken 0.39mm apart and 0.24mm apart. We can see that by taking the samples closer together, the spatial resolution of the measurements is increased.

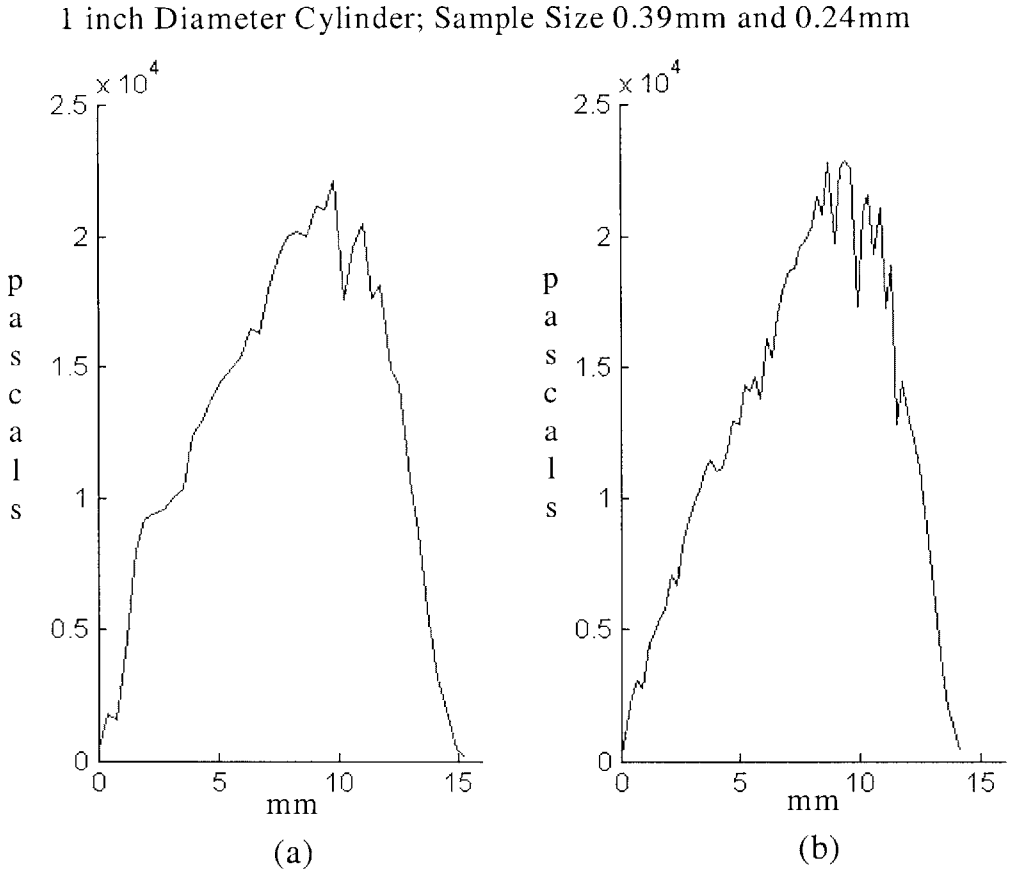

Figure 4-9. Pressure distribution measurement of subject 1 using a 1 inch cylinder with a net force of approximately 1.50N. The samples were taken a) 0.39mm apart and b) 0.24mm apart.

Figure 4-10 shows the results of applying a net force of approximately 1.0N to the finger pad of subject 1 with the 1 inch diameter indentor. The samples were taken 0.039mm apart. Although there is more apparent noise in the measurement, we can see that spatial resolution of the pressure measurement is enhanced, as the finger ridges seem to become more pronounced. However, comparison of the spatial response profile (Figure 3-20) to the data suggests that features less than ~1mm wide may be artifacts due to the bumpy spatial response profile of the sensor.

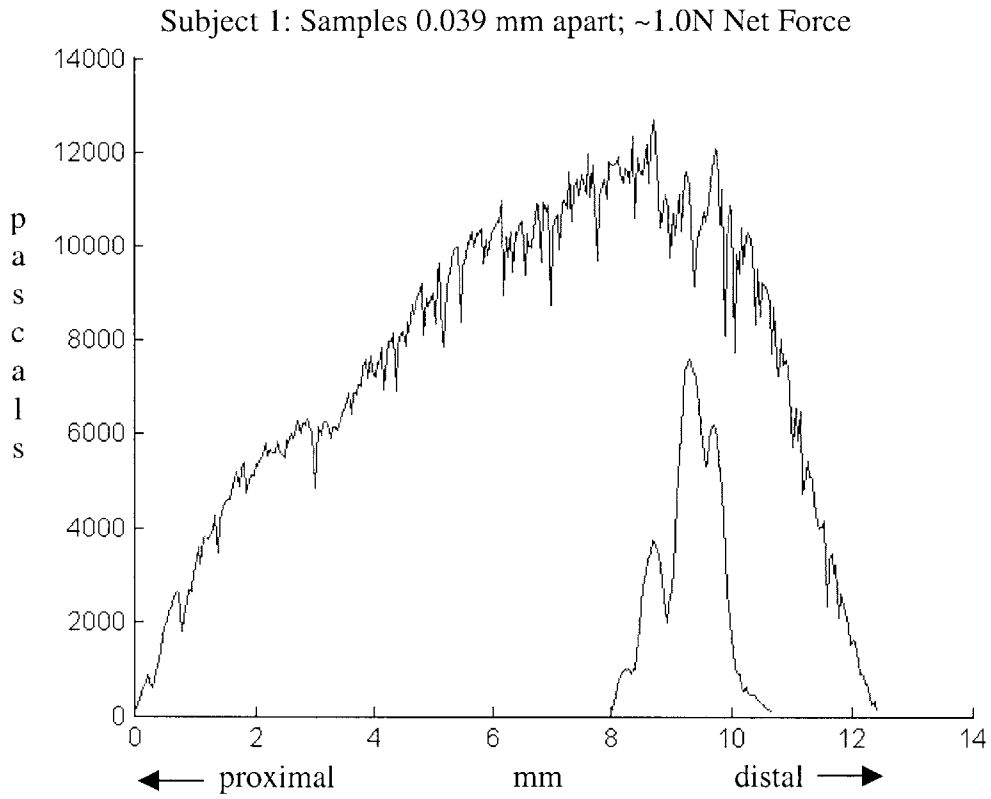

Figure 4-10. Pressure distribution measurement of subject 1 using a 1 inch cylinder with a net force of 1.0N. Samples were taken 0.039mm apart. The spatial response profile of the pressure sensor is also plotted.

It would be useful to correlate these apparent finger ridges in the pressure measurement with the finger ridges in the finger pad. To investigate this correlation, we first took the pressure distribution measurements from the finger pad of subject 1, then wrapped a piece of paper around the sensor while it was attached to the indentor. We then applied ink to the subject's finger, and applied the indentor to the finger pad with the same total force used during the pressure distribution measurements. The resulting fingerprint, shown in Figure 4-11, was then used to correlate the possible finger ridges seen in the pressure distribution with the pattern of ridges on the subject's skin. Figure 4-12 shows the pressure distribution measurement along with vertical lines that roughly correspond to the location of the grooves in the fingerprint.

Figure 4-11. Fingerprint of subject used to correlate with the possible finger ridges seen in the pressure distribution measurement.

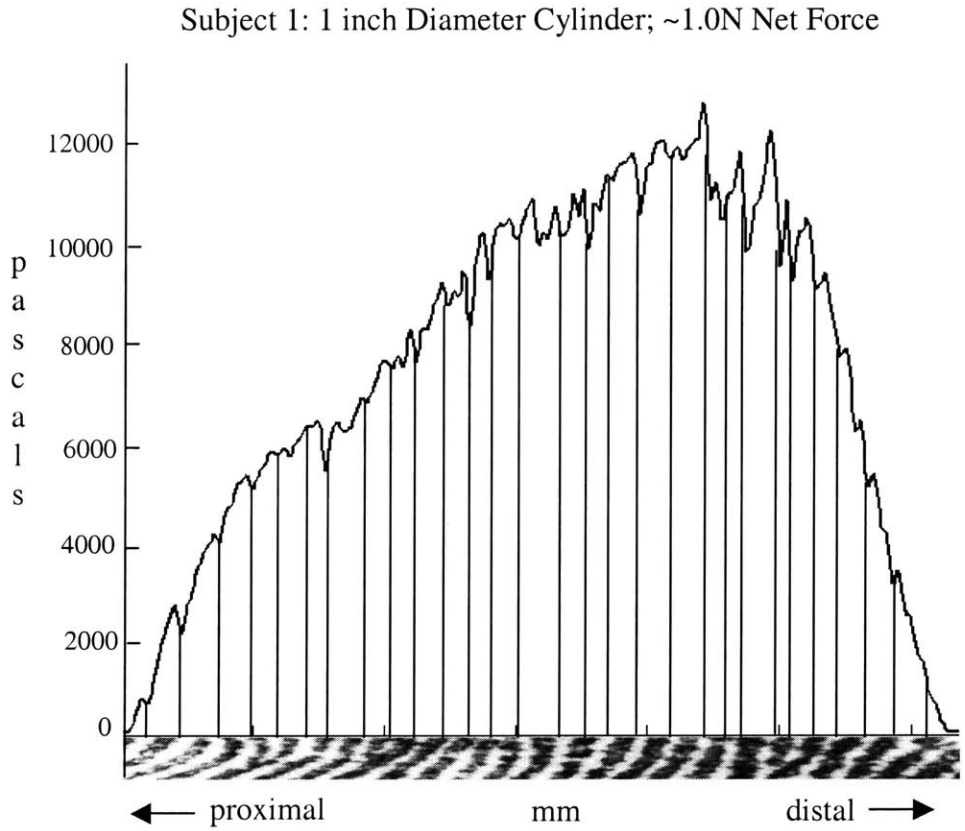

Figure 4-12. Pressure distribution measurement of subject 1 using a 1 inch cylinder with a net force of approximately 1.0N. The vertical lines correspond approximately to the location of the grooves in the fingerprint. The strip indicates the portion of the fingerprint scanned by the sensing element.

4.3 Comparison to Hertz Theory Predictions

Hertz theory (reviewed in Chapter 2) provides a rough approximation the finger pad pressure distribution. Figure 4-13 compares the pressure distribution predicted by Hertz theory to pressures measured under a 1 inch diameter cylinder exerting a net force of 0.5116N. The magnitude and width of the Hertz pressure agree with observed values to within about 10% in the middle of the contact area, but fall off too quickly near the edges.

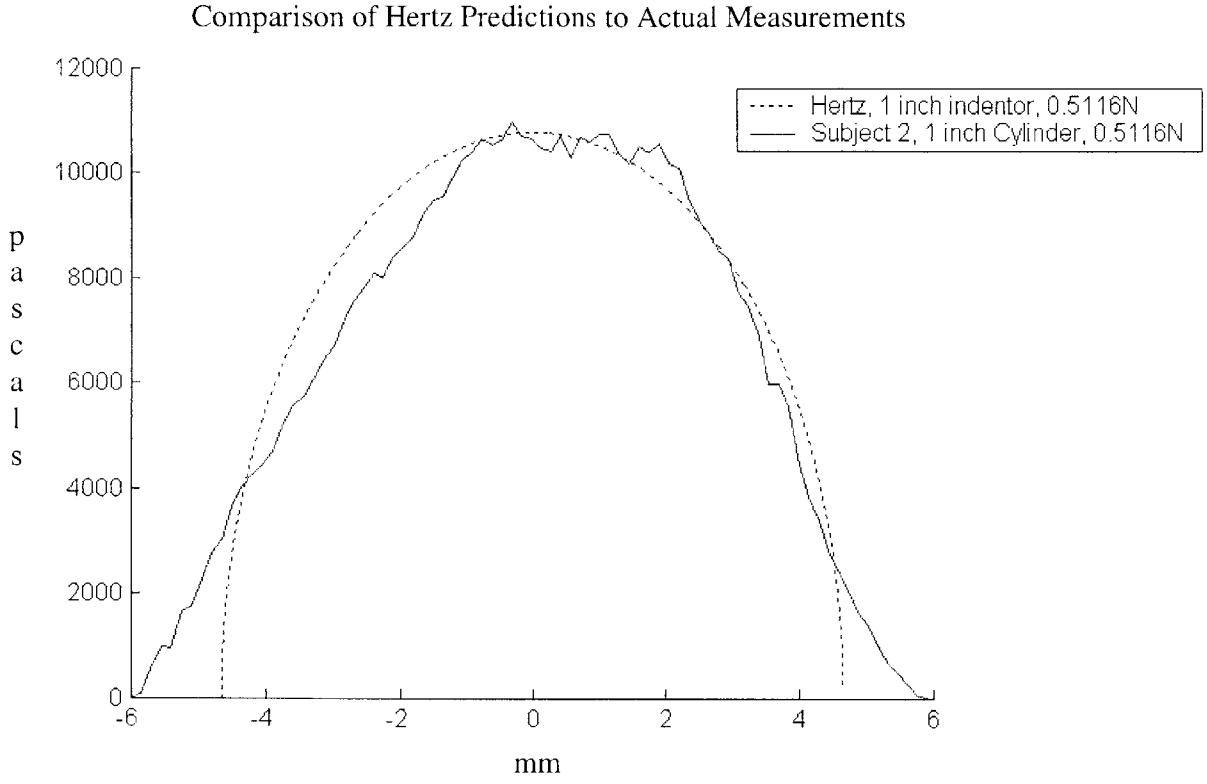

Figure 4-13. Comparison of the pressure distribution measured for a 1 inch diameter cylinder with a load of 0.5116N (solid line) to the pressure distribution predicted by Hertz Theory (dashed line).

Figure 4-14 compares the pressure distribution predicted by Hertz theory to our pressure measurement for a ½ inch diameter cylinder and a load of 0.5498N. The peak magnitude and width of the pressure measurement predicted by Hertz theory are relatively close to

the observed pressure distribution. However, Hertz theory fails to model the observed asymmetry of the pressure distribution.

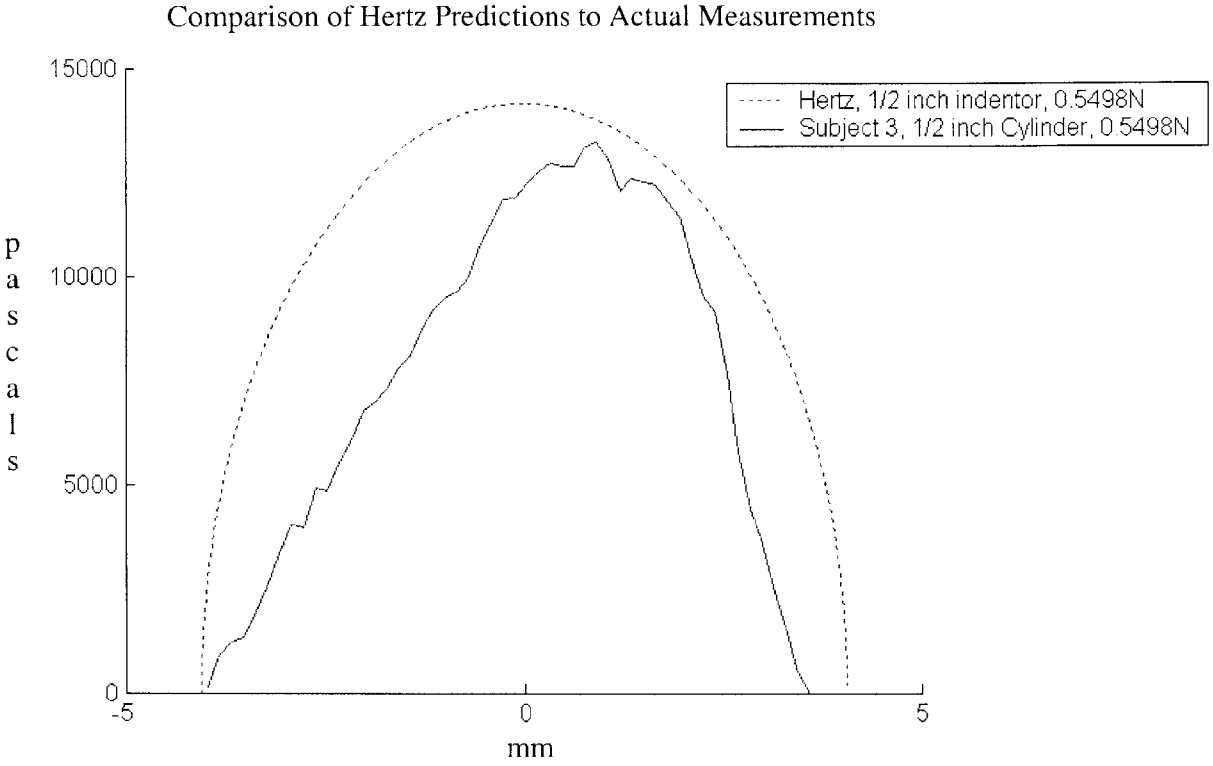

Figure 4-14. Comparison of the pressure distribution measured under a ½ inch diameter cylinder with a load of 0.5498N (solid line) to the pressure distribution predicted by Hertz Theory (dashed line).

4.4 Deconvolution of Pressure Measurements

In order to compute the deconvolution of empirical pressure measurements, the spatial response profile of the pressure sensor was modeled as half of a Gaussian. Figure 4-15 shows the results of applying deconvolution to the pressure measurement result of subject 1 under a 1.0N net force. The spatial resolution of the pressure measurement was slightly increased as a result of the use of deconvolution, by assuming an unrealistically small standard deviation of 0.055mm for the Gaussian half. The general shape is the same but the magnitude of the peaks where finger ridges possibly appear in the pressure record is increased. Unfortunately, attempts to deconvolve the data using half of a Gaussian with

standard deviations closer to that observed in Figure 3-20 ($\sigma \cong 0.5$mm), resulted in estimates of the pressure signal that were grossly in error. Using the raw spatial response profile shown in Figure 3-20 also produced poor results. Low pass filtering the data and spatial response profile did not fix the problem.

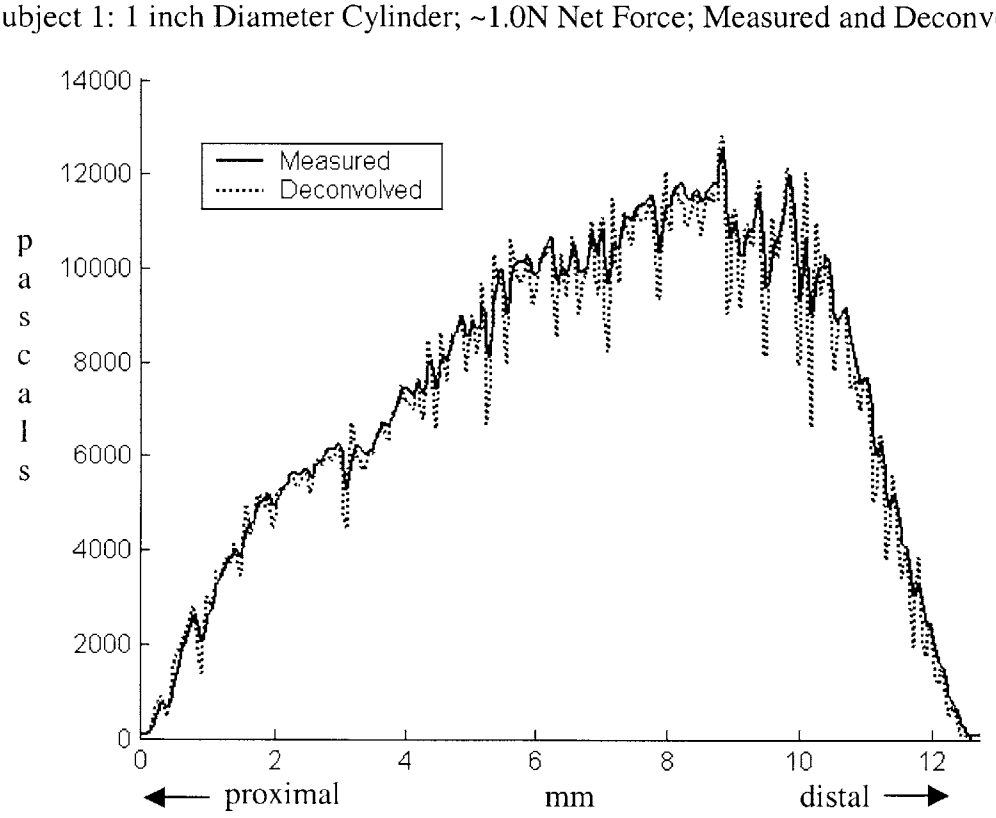

Figure 4-15. The measured (solid line) and deconvolved (dotted line) pressure distribution measurement for a 1 inch diameter cylinder with a net force of approximately 1.0N.

Figure 4-16 shows the results of applying deconvolution to the pressure measurements from subject 5 with a 0.50N load from a 1 inch diameter cylinder. The deconvolved signal appears to increase the spatial resolution of the pressure measurement. Again, the general shape and magnitude of the pressure distribution is the same after deconvolution is used. The magnitude of the peaks where finger ridges possibly appear in the pressure records is increased as well.

Subject 5: 1 inch Diameter Cylinder; ~0.50N Net Force; Measured and Deconvolved

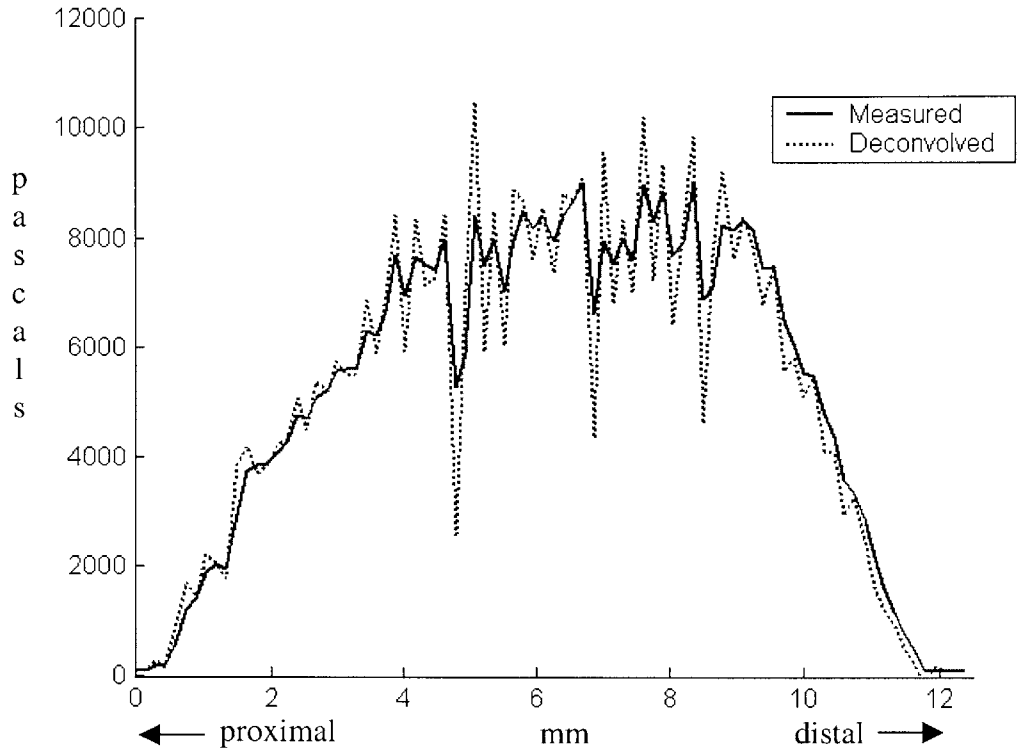

Figure 4-16. The measured (solid line) and deconvolved (dotted line) pressure distribution measurement for a 1 inch diameter cylinder with a load of 0.50N.

5.0 Summary

The surface pressure distribution of the finger pad is important because it is the input to the human tactile system. In this study we explored the relationship between the surface pressure distribution and the shape of contacting objects. We measured the pressure distribution on the surface of the finger in contact with an object using a highly sensitive pressure sensor. The effects of curvature and downward displacement on our surface pressure measurements were examined. We then used deconvolution to increase the spatial resolution of the empirical data.

A motion system along with a pressure sensor was used investigate the surface pressure of the finger pad. The behavior of the pressure sensor was examined to understand its characteristics and limitations. Drift, repeatability, linearity, anisotropy, inter-element variability, and the spatial response profile of the sensor elements were all measured. We showed that the sensor readings are approximately linear, anisotropic, and that the gain for each element of the sensor is different. The spatial response profile was measured and the sensor was calibrated in order to convert readings from voltage to pressure.

The surface pressure was measured from the finger pads of five subjects using both a 1 inch and ½ inch diameter cylinder under various loads. The spacing between samples was varied to see if a smaller step size between measurements produced better results. The correlation between pressure records and the fingerprint of one subject was explored. We found that the dips in the surface pressure record correlated approximately with the pattern of grooves in the finger print. The pressure records were compared with the pressure distribution as predicted by Hertz theory, and the overall shape and magnitude of the predicted and measured pressure distribution were found similar.

Deconvolution was used to increase the spatial resolution of the measurements. Using an unrealistic model for the spatial response profile enabled a slight increase in the spatial resolution of the pressure measurements, but not to the degree that was hoped for. This was most likely due to sensor noise, and the complexity of the spatial response profile.

References

Bicchi, A., Scilingo E., and Rossi, D., "Haptic Discrimination of Softness in Teleoperation: The Role of the Contact Area Spread Rate," *IEEE Transactions on Robotics and Automation*, 16(5): 496-504, **October 2000**.

Birch, A.S. and Srinivasan, M.A., "Experimental Determination of the Viscoelastic Properties of the Human Fingerpad," Touch Lab Report, *RLE Technical Report – 632*, MIT, **1999**.

Bloom, W. and Fawcett, D. *A Textbook of Histology*. W. B. Saunders Company, Philadelphia, pp. 563-580, **1975**.

Cysyk, J. "Skin Dynamics in the Tactile Sensing of Shape", Dept. of Electrical Engineering, MIT September, **1999**.

Dandekar, K. and Srinivasan, M.A., "Role of Mechanics in Tactile Sensing of Shape," Touch Lab Report 2, *RLE Technical Report – 604*, MIT, **1996**.

Darian-Smith, I. "The Sense of Touch: Performance and Peripheral Neural Processes," *Handbook of Physiology – The Nervous System –III*, pp. 739-788, **1984**.

Diller, T. T., "Frequency Response of Human Skin in Vivo to Mechanical Stimulation," S. M. Thesis., Dept. of Mechanical Engineering, MIT, **2001**.

Fearing, R.S. "Tactile Sensing Mechanisms," *International Journal of Robotic Research*, 9:3-23, **1990**.

Fearing, R.S., and Hollerback, J.M., "Basic Solid Mechanics for Tactile Sensing," *International Journal of Robotic Research*, Vol. 4, No. 3, **Fall 1985**.

Goodwin, A. W., John, K. T., and Marceglia, A. H., "Tactile discrimination of curvature by humans using only cutaneous information from the fingerpads," *Experimental Brain Research*, vol. 86, pp. 663-672, **1991**.

Goodwin, A. W. and Wheat, H. E., "Human tactile discrimination of curvature when contact area with the skin remains constant," *Experimental brain research*, vol. 88, pp. 447-450, **1992**.

Gulati, R. and Srinivasan, M., "Determination of Mechanical Properties of the Human Fingerpad, *in vivo*, using a Tactile Simulator," *RLE Technical Report – 606*, MIT, **1996**.

Hajian, A. Z. and Howe, R. D., "Identification of the mechanical impedance at the human finger tip," *ASME Journal of Biomechanical Engineering*, 119(1), pp. 109-114, **February 1997**.

Ho, C. -H. and Srinivasan, M., "Human Haptic Discrimination of Thickness," *RLE Technical Report – 608*, MIT, **1996**.

Hodgkin, A. L. and Huxley, A. F., "A quantitative description of membrane current and its application to conduction and excitation in nerve," *Journal of Physiology*, pp. 117-500, **1952**.

Howe, R. S. and Cutkosky, M. R., "Dynamic Tactile Sensing: Perception of Fine Surface Features with Stress Rate Sensing," *IEEE Transactions on Robotic and Automation*, vol. 9, no. 2, pp. 140-151, **1993**.

Johansson, R.S. and Vallbo, A.B., "Tactile sensory coding in the glabrous skin of the human hand," *Trends in Neuroscience*, vol. 6, pp. 27-32, **January 1983**.

John, K. T., Goodwin, A. W., and Darian-Smith, I., "Tactual discrimination of thickness," Experimental brain research, vol. 78, no. 1, pp. 62-68, **1989**.

Johnson, K.L. *Contact Mechanics*. Cambridge University Press, Great Britain, **1985**.

Karason, S. P., Annaswamy, A., and Srinivasan, M. A., "Identification and Control of Haptic Systems: A Computational Theory," *RLE Technical Report – 621*, MIT, **1998**.

Karason, S. P., Srinivasan, M. A., and Annaswamy, A., "Encoding and Decoding of Static Information in Tactile Sensing Systems," *The International Journal of Robotics Research*, vol. 18, no. 2, pp. 131-151, **February 1999**.

Karu, Z. Z., *Signals and Systems Made Ridiculously Simple*, ZiZi Press, Cambridge, Massachusetts, **1995**.

Lamb, G. D., "Tactile discrimination of textured surfaces: Psychophysical performance measurements in humans," *Journal of Physiology (London)*, vol. 338, pp. 551-565, **1983**.

Lanir, Y., Dikstein, S., Hartzshtark, A., and Manny, V., "*In Vivo* Indentation of Human Skin," *Journal of Biomechanics*, vol. 112, pp.63-69, **1990**.

Lederman, S. J. and Taylor, M. M., "Fingertip force, surface geometry, and the perception of roughness by active touch," *Perception & Phychophysics*, vol. 12, pp. 401-408, **1972**.

Liao, J. C. and Srinivasan, M. A., "Experimental Investigation of Frictional Properties of the Human Finger Pad," *RLE Technical Report – 629*, MIT, September, **1999**.

Lockhart, R. D., Hamilton, G. F., and Fyfe, F. W., *Anatomy of the Human Body*, JP Lippincott Co., Philadelphia, **1965**.

Maeno, T., Kobayashi, K, and Yamazaki, N., "Relationship Between the Structure of Human Finger Tissue and the Location of Tactile Receptors," *JSME International Journal*, Series C, Vol. 41, No. 1, **1998**.

NuDAQ, *ACL-8111 Multi-Function Data Acquisition Card Users Manual*, ADLink Technologies Inc., Rev. 2.2, **January 1999**.

Pawluk, D. T. V., "A Visocelastic Model of the Human Fingerpad and a Holistic Model of Human Touch," Ph.D. Thesis, Harvard University, May **1997**.

Pawluk, D. T. V. and Howe, R. D., "Dynamic contact of the human fingerpad against a flat surface," *ASME Journal of Biomechanical Engineering*, 121(6), pp. 605-611, **December 1999**.

Pawluk, D. T. V. and Howe, R. D., "Dynamic Lumped Element Response of the Human Fingerpad," *ASME Journal of Biomechanical Engineering*, 121(2), pp. 178-184, **April 1999**.

Pawluk, D. T. V., Son, J. S., Wellman, P. S., Peine, W. J, and Howe, R. D., "A Distributed Pressure Sensor for Biomechanical Measurements," *ASME Journal of Biomechanical Engineering*, 102(2), pp. 302-305, **April 1998**.

Phillips, J. R. and Johnson, K. O., "Tactile Spatial Resolution – II. Neural Representation of Bars, Edges and Gratings in Monkey Primary Afferents," *J. Neurophysiol*, vol. 46, pp. 1192-1203, **1981a**.

Phillips, J. R. and Johnson, K. O., "Tactile Spatial Resolution – III. A Continuum Mechanics Model of Skin Predicting Mechanoreceptor Responses to Bars, Edges and Gratings," *J. Neurophysiol*, vol. 46, pp. 1204-1225, **1981b**.

Pressure Profile Systems, Inc., "TactArray: Tactile Array Systems," *http://www.pressureprofile.com*, **July 2002.**

Raju, B and Srinivasan MA, "Encoding and Decoding of Shape in Tactile Sensing," Touch Lab Report 12, *RLE Technical Report - 630*, MIT, **1999**.

Serway, R., *Physics*, Saunders College Publishing, Philadelphia, 3rd. Edition, pp. 1074-1082, **1990**.

Srinivasan, M. A., "Surface Deflection of Primate Fingertip Under Line Load," *J. Biomechanics*, vol. 22, no. 4, pp. 343-349, **1989**.

Srinivasan, M. A. and Dandekar, K. "An Investigation of the Mechanics of Tactile Sense using Two-Dimensional Models of the Primate Fingertip," *J. Biomechanical Engineering*, vol. 118, pp. 48-55, **1996**.

Srinivasan, M. A. and LaMotte, R. H., "Encoding of Shape in the Response of Cutaneous Mechanoreceptors," *Information Processing in the Somatosensory System*, Franzen and Westman, Wenner-Gren International Symposioum Series, MacMillan Press, pp. 59-69, **1991**.

Srinivasan, M. A. and LaMotte, R. H., "Tactual Discrimination of Softness," *J. Neurophysiology*, vol. 73, no. 1, pp. 88-101, **1995**.

Srinivasan, M. A., Whitehouse, J. M, and LaMotte, R. H., "Tactile detection of slip: Surface microgeometry and peripheral neural codes," *Journal of Neurophysiology*, vol. 63, no. 6, pp. 1323-1332, **1990**.

Tregear, R. T., *Physical Functions of Skin*, Academic Press, New York, **1966**.

Tubiana, R., *The Hand*, W.B. Saunders Company, Philadelphia, **1981**.

Voss, K.J. and Srinivasan, M.A., "Investigation of the Internal Geometry and Mechanics of the Human Fingerpad, *in vivo*, using Magnetic Resonance Imaging," Touch Lab Report 10, *RLE Technical Report – 622*, MIT, **1998**.

Williams, P.L., *Gray's Anatomy*, Churchill Livingstone, New York, pp. 375-398, Third Edition, **1995**.